Title

New factors for protein transport identified by a genome-wide CRISPRi screen in mammalian cells

Journal

Journal of Cell Biology, 218(11)

ISSN

0021-9525

Authors

Bassaganyas, Laia

Popa, Stephanie J

Horlbeck, Max

et al.

Publication Date

2019-11-04

DOI

10.1083/jcb.201902028

Peer reviewed

JCB Journal of Cell Biology

TOOLS

New factors for protein transport identified by a genome-wide CRISPRi screen in mammalian cells

Laia Bassaganyas[1], Stephanie J. Popa[2], Max Horlbeck[3], Claudia Puri[4], Sarah E. Stewart[2], Felix Campelo[5], Anupama Ashok[6], Cristian M. Butnaru[6,7], Nathalie Brouwers[6], Kartoosh Heydari[8], Jean Ripoche[9], Jonathan Weissman[3], David C. Rubinsztein[4,10], Randy Schekman[11], Vivek Malhotra[6], Kevin Moreau[2*], and Julien Villeneuve[2,4*]

Protein and membrane trafficking pathways are critical for cell and tissue homeostasis. Traditional genetic and biochemical approaches have shed light on basic principles underlying these processes. However, the list of factors required for secretory pathway function remains incomplete, and mechanisms involved in their adaptation poorly understood. Here, we present a powerful strategy based on a pooled genome-wide CRISPRi screen that allowed the identification of new factors involved in protein transport. Two newly identified factors, TTC17 and CCDC157, localized along the secretory pathway and were found to interact with resident proteins of ER-Golgi membranes. In addition, we uncovered that upon TTC17 knockdown, the polarized organization of Golgi cisternae was altered, creating glycosylation defects, and that CCDC157 is an important factor for the fusion of transport carriers to Golgi membranes. In conclusion, our work identified and characterized new actors in the mechanisms of protein transport and secretion and opens stimulating perspectives for the use of our platform in physiological and pathological contexts.

Introduction

The molecular machinery underlying the processes of protein transport and secretion has been conserved from yeast to mammalian cells, being essential to maintain specificity and communication between organelles, exocytosis, and endocytosis. Fully one third of proteins navigate the secretory pathway, entering this system via the ER. They are then transported via cellular compartments, including the Golgi apparatus and transport carriers, to be targeted to their final destination (Lee et al., 2004). Recent demonstrations indicate that cell compartments establish cross-regulatory mechanisms through numerous membrane contact sites (Wu et al., 2018), are endowed with tightly regulated dynamics (Valm et al., 2017), and stand at the crossroad of signaling pathways where inputs and outputs are integrated and coordinated (Luini and Parashuraman, 2016). Thus, protein transport and secretion processes are clearly more complex than previously thought.

Yeast genetic studies and in vitro biochemical approaches were initially used to discover the basal protein transport machinery (Novick et al., 1980; Braell et al., 1984). More recently, arrayed RNA interference screens at the genome scale or targeting kinases/phosphatases expanded the list of functional and regulatory components of secretory pathways in metazoan cells (Bard et al., 2006; Asensio et al., 2010; Wendler et al., 2010; Chia et al., 2012; Simpson et al., 2012). In these studies, artificial secreted reporters preceded by a signal sequence such as HRP (ss-HRP) or firefly luciferase were used for detection (Bard et al., 2006; Wendler et al., 2010). Alternatively, secretory pathway organization or transport to the cell surface of fluorescently labeled exogenous transmembrane proteins such as vesicular stomatitis virus G (VSV-G) were analyzed using high throughput imaging or flow cytometry systems (Asensio et al., 2010; Chia et al., 2012; Simpson et al., 2012). Although these approaches were useful, their implementations in different cell types, with

[1]Department of Medical Genetics, National Institute for Health Research Cambridge Biomedical Research Centre, and Cancer Research UK Cambridge Centre, University of Cambridge, Cambridge, UK; [2]University of Cambridge Metabolic Research Laboratories, Wellcome Trust–Medical Research Council Institute of Metabolic Science, University of Cambridge, Cambridge, UK; [3]Department of Cellular and Molecular Pharmacology, University of California, San Francisco, San Francisco, CA; [4]Department of Medical Genetics, Cambridge Institute for Medical Research, University of Cambridge, Cambridge, UK; [5]Institut de Ciencies Fotoniques, Barcelona Institute of Science and Technology, Castelldefels, Spain; [6]Centre for Genomic Regulation, Barcelona Institute of Science and Technology, Barcelona, Spain; [7]Department of Photonic Investigations, Center of Advanced Laser Technologies, National Institute for Laser, Plasma and Radiation Physics, Magurele, Romania; [8]Cell Therapy Facility, Stanford Health Care, Stanford, CA; [9]Institut National de la Sante et de la Recherche Medicale U1026, Université de Bordeaux, Bordeaux, France; [10]UK Dementia Research Institute, Cambridge, UK; [11]Department of Molecular and Cell Biology, Howard Hughes Medical Institute, University of California, Berkeley, Berkeley, CA.

*K. Moreau and J. Villeneuve contributed equally to this paper; Correspondence to Julien Villeneuve: julienvilleneuve81@gmail.com; K. Moreau's present address is Oncology Safety, Pharmaceutical Sciences, Research and Development, AstraZeneca, Cambridge, UK.

various cargo proteins and environmental conditions, remain difficult.

Indeed, a current challenge is to understand how secretory pathways are adapted and regulated in response to intrinsic demands or environmental cues, and eventually altered in diseases. Toward this objective, versatile platforms are needed to uncover factors involved in protein transport in various physiological and pathophysiological contexts. Recent developments of the bacterial CRISPR-associated nuclease Cas9 technology paired with libraries of single-guide RNAs (sgRNAs) have been successfully used to perform pooled genome-wide screening (Shalem et al., 2015; Kampmann, 2018), where targeted genes can be disrupted (Shalem et al., 2014) and gene expression can be inhibited or activated (Gilbert et al., 2014).

Here, we developed an efficient strategy using a pooled genome-wide CRISPR interference (CRISPRi) screen to identify genes involved in protein trafficking and secretion in mammalian cells, and we highlight the contribution of newly identified factors in these processes.

Results

Dual fluorescent reporter for protein transport

We first established a HeLa cell line stably expressing the GFP-tagged TAC protein (interleukin-2 receptor) and the catalytically inactive Cas9 (dCas9) fused to the KRAB repressor protein (HeLa TAC-GFP dCas9-KRAB cells). The TAC protein, which contains a single transmembrane domain (TMD) and localizes at the cell surface, represents a straightforward reporter to investigate protein transport along the ER-Golgi secretory pathway (Stanley and Lacy, 2010). A GFP signal allows monitoring of the total expression of the TAC protein, whereas its cell surface expression can be assessed by immunofluorescence microscopy and flow cytometry analysis using a phycoerythrin (PE)–conjugated antibody, which recognizes the extracellular domain of the TAC protein (Fig. 1, A–C; and Fig. S1). On the other hand, the dCas9-KRAB fusion protein in association to sgRNA targeting the transcription start site (TSS) of specific genes (CRISPRi system) is a powerful tool to inhibit gene expression (Gilbert et al., 2013). We first tested our reporter system by incubating cells with brefeldin A (BFA), an inhibitor of protein transport through the ER and Golgi membranes (Misumi et al., 1986). Flow cytometry analysis demonstrated a decrease of TAC surface expression upon BFA treatment (Fig. 1 D). Incubation of cells with trypsin, a protease that cleaves most proteins expressed at the cell surface, strongly reduced TAC surface expression that recovered after 18 h in trypsin-free medium. In these conditions, BFA treatment prevented TAC surface expression recovery (Fig. 1 E).

We then validated our cell line by analyzing TAC expression after knockdown of genes essential for secretory pathway function. Cells were infected with lentivirus to express control sgRNA (Gal4) or sgRNAs targeting the TSS of *SCFD1*, which regulates SNARE complex assembly (Carr and Rizo, 2010), *Sec24A*, a COPII vesicular coat subunit (Wendeler et al., 2007), or *Sec61A*, which promotes translocation of secreted and membrane proteins into the ER (Voorhees and Hegde, 2016). A tight quality control is associated with the cotranslational insertion of nascent polypeptide chains upon emergence from the ribosomal exit tunnel, and a translocation defect of nascent polypeptide chains in the ER leads to their degradation (Brandman and Hegde, 2016). For this reason, down-regulation of Sec61A is an appropriate control to monitor TAC expression when TAC translation is altered. 7 d after infection, total and surface TAC expressions were monitored by flow cytometry. Sec61A knockdown, as expected, reduced both surface and total TAC expression. However, SCFD1 and Sec24A knockdown strongly reduced TAC surface transport without affecting the total TAC expression (Fig. 1, F and G). Cells were also analyzed for the surface/total TAC expression ratio. Upon SCFD1 and Sec24A knockdown, a strong enrichment in the lower quartile was observed related to a decrease of TAC surface expression. Interestingly, no enrichment in one or the other quartile was detected in Sec61A-depleted cells, where both surface and total TAC expression were reduced (Fig. 1, G and H). Altogether, these results established our cell line as an efficient and specific cellular platform to monitor secretory pathway function, and prompted us to use it to perform a pooled genome-wide CRISPRi screen.

Genome-wide CRISPRi screen mostly identifies genes involved in protein transport

HeLa TAC-GFP dCas9-KRAB cells were transduced with the CRISPRi-v2 library (Horlbeck et al., 2016a) at a low MOI (0.3) and selected for stable integration with puromycin. 7 d after transduction, cells were separated by FACS into a high and low surface/total TAC expression ratio, selecting upper and lower quartiles, respectively. Genomic DNA was then isolated, and read counts of sgRNAs were obtained by deep sequencing to determine the abundance of each sgRNA in the two cell fractions (Fig. 2 A). Subsequent analysis using MAGeCK (Li et al., 2014) allowed the identification of many genes whose down-regulation modified TAC transport at the cell surface (Table S1 and Fig. 2 B).

On one hand, in the lower quartile, gene ontology term enrichment analysis of the 100 top-ranked genes revealed that knockdown of genes encoding components of "Golgi vesicle transport" was the main functional category inhibiting TAC transport (Fig. 2, B and C). Genes involved in "toxin transport," "antigen processing and presentation," and "Golgi organization" were also highly enriched. More specifically, we identified as top hits most of the COPI subunits (COPA, COPB1, COPB2, COPG1, COPZ1, and ARCN1) as well as the COPII subunits Sec24A, Sec24B, and Sec13. We also identified the SNARE Sec22B and the SNARE-associated factors SCFD1 and NBAS, several subunits of the TRAPP complex and the conserved oligomeric Golgi complex, the small GTPase SAR1 and the Rab GTPase RAB1A, the Sec23-interacting protein Sec23IP, and the exocyst complex component EXOC2, among others (Table S1 and Fig. 2 B). Interestingly, factors belonging to small ADP-ribosylation factor (ARF) and ADP-ribosylation factor-like (ARL) GTPases, Golgins, or additional SNAREs were not identified among the top hits. This is consistent with previous reports (Wendler et al., 2010;

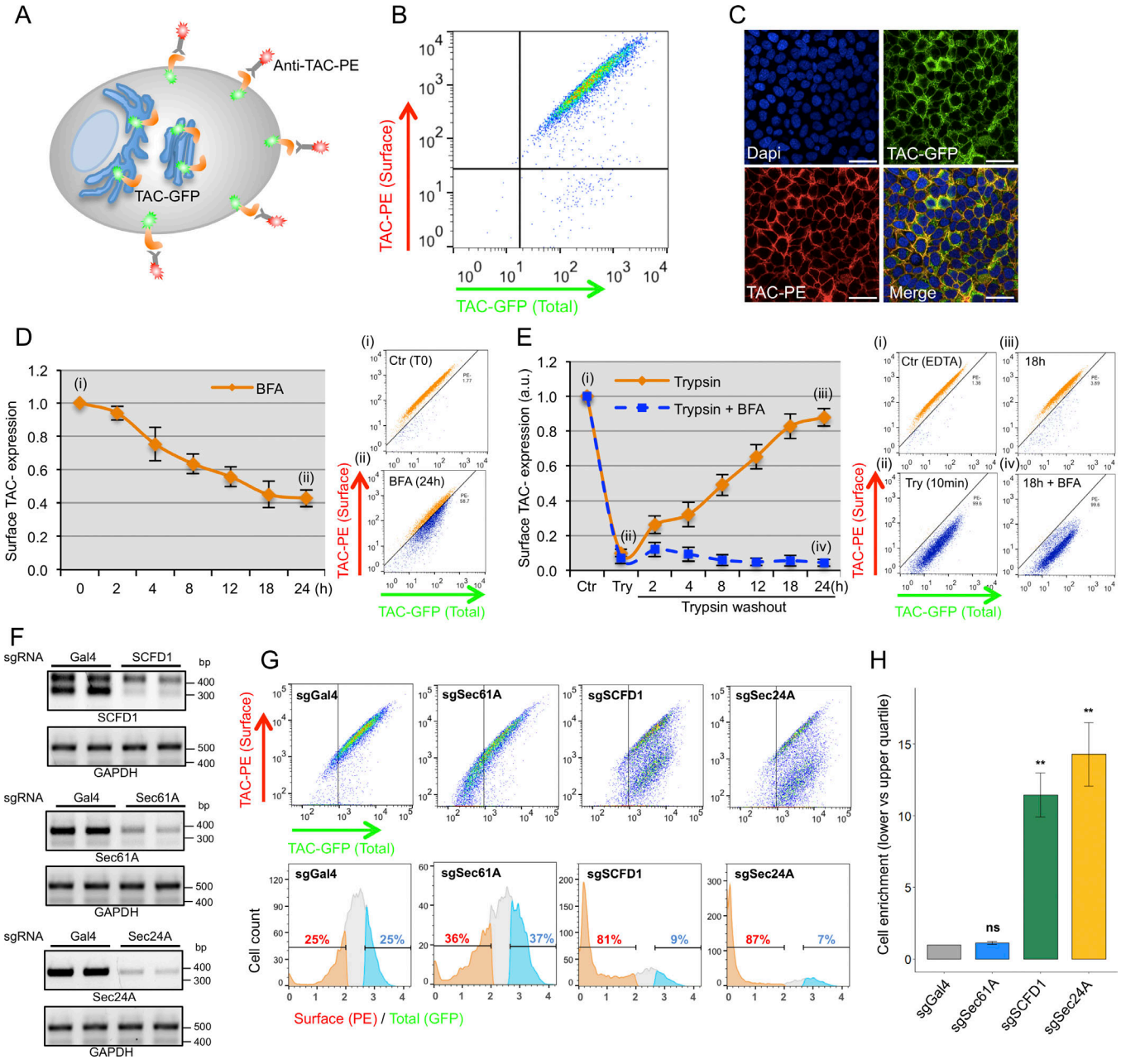

Figure 1. **Dual fluorescent reporter for protein transport. (A)** Schematic representation of the reporter based on HeLa TAC-GFP cells. **(B and C)** Surface and total TAC expressions in HeLa TAC-GFP cells were analyzed by flow cytometry (B) and immunofluorescence microscopy (C). Nuclei were stained with DAPI. Scale bars, 50 µm. **(D)** HeLa TAC-GFP cells were incubated in presence of 500 ng/ml BFA for the indicated times, after which cells were washed with PBS and detached by incubation in PBS containing 0.5 mM EDTA, and surface and total TAC expressions were analyzed by flow cytometry. **(E)** HeLa TAC-GFP cells were detached after incubation with 0.5 mM EDTA (Control, Ctr [i]) or with trypsin (Try [ii]), and then cells were plated in complete medium in the absence (iii) or presence (iv) of 500 ng/ml BFA. At indicated times, surface and total TAC expressions were analyzed by flow cytometry. In D and E, surface TAC expression was calculated relative to the total expression as the ratio of the mean of fluorescence intensities and normalized to control sample (mean of $n = 3 \pm$ SEM). **(F)** HeLa TAC-GFP dCas9-KRAB cells were infected with lentivirus to express control sgRNA (Gal4) or sgRNAs targeting the TSS of *SCFD1*, *Sec24A*, and *Sec61A*. 7 d after infection, the knockdown efficiency of targeted genes was monitored by RT-PCR. **(G)** Surface and total TAC expressions (top panels) and surface/total TAC expression ratio (bottom panels) were analyzed by flow cytometry in control HeLa TAC-GFP dCas9-KRAB cells and in cells depleted for Sec61A, SCFD1, or Sec24A. In bottom panels, lower and upper quartiles are set on control cells and applied to the other experimental conditions. **(H)** Quantification of the enrichment of cells in the lower quartile compared with the upper quartile as presented in G, bottom panels (mean of $n = 4 \pm$ SEM; two-tailed Student's *t* test for comparison to control condition sgGal4; **, $P < 0.01$; ns, statistically nonsignificant).

Simpson et al., 2012), highlighting the high degree of redundancy between paralog genes that could explain why the knockdown of these components did not alter robustly TAC transport. Of note, genes involved in mRNA homeostasis and protein translation were also identified among hit genes. Although it is likely that their knockdown indirectly alters TAC

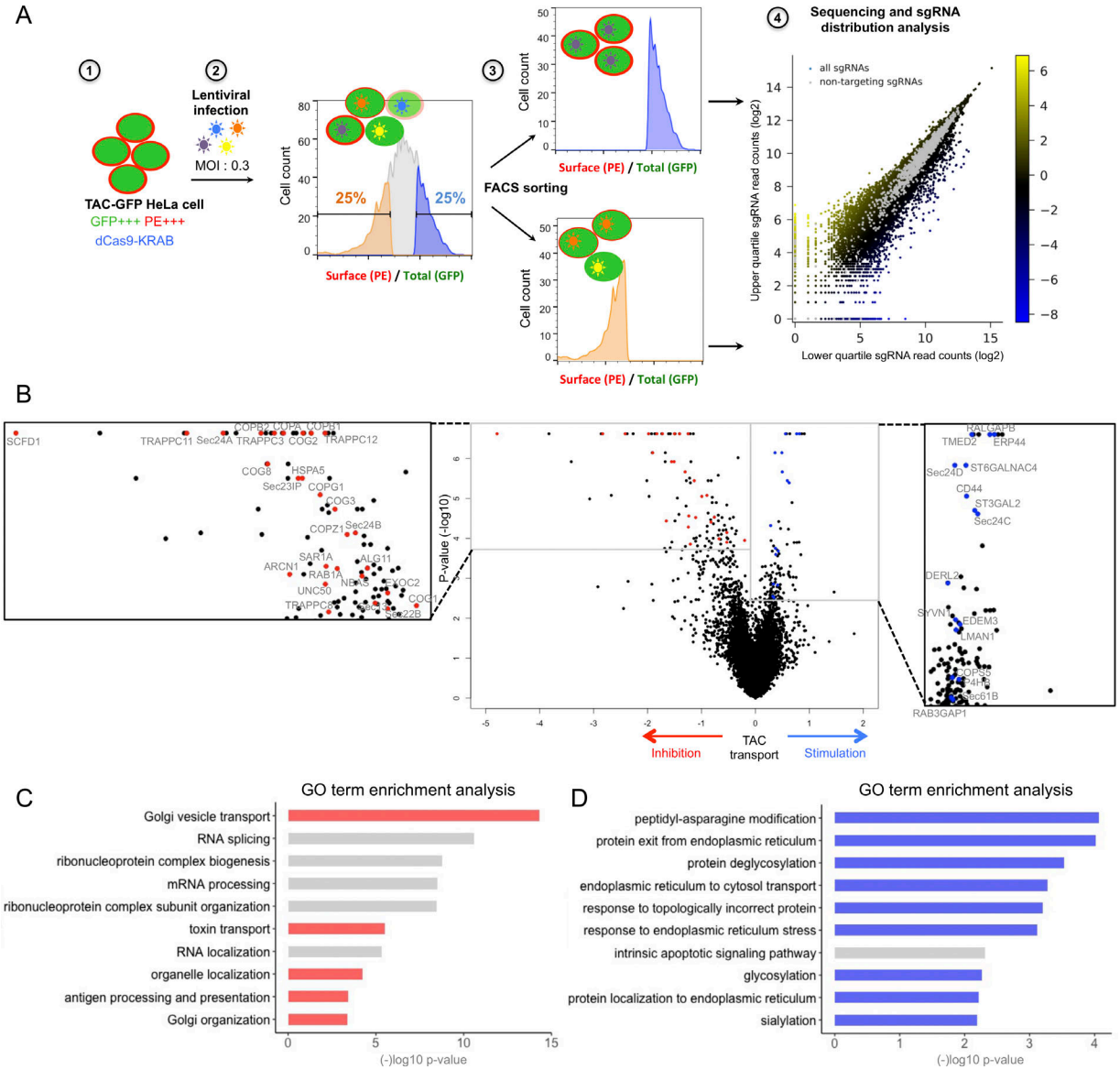

Figure 2. **Pooled genome-wide CRISPRi screen for protein transport. (A)** Schematic representation of the pooled CRISPRi screening workflow. HeLa TAC-GFP dCas9-KRAB cells (1) were infected with the CRISPRi-v2 library (2). Then, using flow cytometry–based sorting, two cell fractions representing a low and high surface/total TAC expression ratio were collected (3), and the abundance of each sgRNA in the two fractions was assessed by sequencing (4). The scatter plot represents the sgRNA read counts (log2) derived from each cell fraction obtained after DNA sequencing. The color bar indicates the values of phenotype (fold change [log2]) obtained for each individual sgRNA. sgRNAs with a phenotype <0 indicate an enrichment in the lower quartile, and sgRNAs with a phenotype >0 indicate an enrichment in the upper quartile. **(B)** Volcano plot showing for each gene, the knockdown effect on TAC transport, and P value (−log10) of phenotype. Screen replicates were averaged. Each gene targeted by the library of sgRNA is indicated with a black dot. Genes included in the 100 top ranked genes (inserts) and belonging to functional categories of interest (highlighted in C and D) are indicated with red dots for genes inhibiting TAC transport and with blue dots for genes stimulating TAC transport. Entire datasets are reported in Table S1. **(C and D)** gene ontology (GO) term enrichment analysis among the 100 top ranked genes whose depletion results in TAC transport inhibition (C) and TAC transport stimulation (D).

transport, a subset of them may also be part of transcriptional or translational programs required for the expression of components specifically involved in the secretory pathway. We can also not exclude the possibility that some of these genes may have additional nonbiosynthetic functions.

On the other hand, in the upper quartile, the knockdown of genes encoding known components involved in "protein exit from the ER," "response to topologically incorrect protein," "ER to cytosol transport," and "response to ER stress," as well as components involved in posttranslational modification, were the main functional categories promoting TAC transport (Fig. 2, B and D). This suggests that inhibition of the machinery required for the maintenance of ER homeostasis and quality control along the secretory pathway may favor transport of cargo proteins that are most likely misfolded or incompletely processed.

Altogether, these results clearly demonstrated the value of our approach to identify genes involved in secretory pathway function and organization.

A secondary screen identifies new factors required for protein transport and secretion

62 genes with unknown or poorly characterized function that were identified either in the lower or upper quartiles as candidate genes (Table S2) were selected for a secondary screen using a secretion assay based on the detection of ss-HRP (von Blume et al., 2009; see Materials and methods for selection criteria of candidate genes). Genes were knocked down in HeLa–ss-HRP after transfection of specific smart pool siRNAs prearrayed in a 96-well plate. After 3 d, cells were washed and incubated with complete medium, and cell lysates and medium were harvested after 8 h for HRP quantification. As a positive control, in SCFD1-depleted cells, a strong signal in the cell lysate associated with a low signal detected in the medium demonstrated a clear defect of HRP secretion resulting in its accumulation inside cells (Fig. 3 A and Table S2). This approach identified several genes for which the knockdown inhibited HRP secretion. They included, for example, *WDR7*, *YPEL5*, *TMEM161*, *FAM162B*, and *GPR162* that encode an orphan G protein coupled receptor (GPCR). Interestingly, we also identified few genes where the knockdown promoted HRP secretion such as *TMEM167A*, *FAM46A*, as well as the ubiquitin specific peptidase *USP32* (Fig. 3 A and Table S2). Future analyses will help to dissect their roles.

We selected four genes for further analysis that encode the coiled-coil domain-containing protein 151 (CCDC151), CCDC157, C10orf88, and the tetratricopeptide repeat protein 17 (TTC17). They were highly enriched in the lower quartile of the CRISPRi screen, their knockdown strongly inhibited HRP secretion, and they encode proteins with a poorly defined or unknown function. First, we aimed to confirm the effect of their knockdown on TAC protein transport. HeLa TAC-GFP cells were transfected with specific individual siRNAs and, after 3 d, knockdown efficiency was monitored by RT-PCR (Fig. 3 B). Flow cytometry analysis revealed that knockdown of the selected genes inhibited TAC expression at the cell surface, confirming that they were true hits (Fig. 3, C and D). We also found that their siRNA-mediated knockdown reduced the transport of the major histocompatibility complex I (MHC-I), an endogenous cargo protein trafficked along the ER-Golgi secretory pathway to the cell surface (Fig. 3, E–G). Altogether, these results demonstrated that the selected candidate genes were required for both exogenous and endogenous cargo protein transport.

The newly identified factors are essential for secretory pathway organization

Next, we assessed the role of newly identified factors on the morphology of ER, ER exit sites, cis Golgi membranes and TGN by immunofluorescence microscopy, using antibodies targeting calnexin (CNX), Sec31A, GM130, and TGN46. As a control, in SCFD1-depleted cells, Golgi membranes were completely fragmented, characterized by GM130- and TGN46-positive punctae dispersed throughout the cytoplasm. Interestingly, this phenotype was also observed after CCDC151 and C10orf88 knockdown (Fig. 4, A–C). Conversely, after TTC17 knockdown, Golgi membranes remained localized in the perinuclear area, but presented as an expanded structure (Fig. 4, A, B, and D). In CCDC157-depleted cells, Golgi membranes exhibited a characteristic ring-shaped organization as observed for both GM130 and TGN46 staining (Fig. 4, A, B, and E). Electron microscopy studies confirmed that Golgi stacks had altered ultrastructure in TTC17-depleted cells, characterized by enlarged and swollen Golgi cisternae, and in CCDC157-depleted cells, most likely caused by accumulated and coalesced transport carriers in close proximity of Golgi membranes (Fig. 4 F). Along with the perturbed Golgi complex architecture, the distributions of ER exit sites were also altered upon candidate gene knockdown (Fig. S2 A), with no obvious changes in the distribution and morphology of the ER (Fig. S2 B).

How could the selected factors play a role in protein transport and secretion, and secretory pathway organization? To address this question, we looked for interacting partners using the BioPlex network, which encompasses results aiming at identifying binding partners of proteins encoded by the human genome (Huttlin et al., 2015, 2017). Interrogation of this resource identified TTC17-interacting proteins, including exclusively ER- and Golgi-resident proteins and cargo proteins transported along the secretory pathway (Fig. 5 A). Interacting partners of CCDC151 include the SNARE-associated protein SNAPIN, GTPase Rab-Like protein 5, and Golgin A5 (Fig. 5 B). Interacting partners of C10orf88 include Rab protein GDI2, clathrin heavy chain, clathrin adaptors accessory protein CCDC91, and plasma membrane proteins NCKAP1 and LILRB4 (Fig. 5 C). The BioPlex resource does not contain a network for CCDC157. Taken together, these data supported a direct role of the selected factors on the secretory pathway function, prompting us to probe their site of action.

A Pfam domain analysis (Finn et al., 2016) or TMHMM software (Krogh et al., 2001) did not predict TMD for the selected factors, whereas the HMMTOP algorithm (Tusnády and Simon, 2001) yielded one TMD for TTC17 (TMHMM and HMMTOP are two transmembrane protein topology prediction methods, based on a hidden Markov model). To assess the subcellular localization of the selected factors, we performed immunofluorescence microscopy on HeLa cells using specific antibodies directed against the endogenous proteins, after permeabilization with digitonin and extensive washing. This procedure allows the removal of soluble cytoplasmic pool of proteins, highlighting their potential association with intracellular compartments. This approach revealed a close proximity between CCDC151 and the centrosomal marker centrin-3 (Fig. 5, D and E). This location is consistent with the interacting partners of CCDC151 revealed by BioPlex and the Golgi membrane phenotype observed in CCDC151-depleted cells (Fig. 4, A and B). Indeed, interacting partners of CCDC151 included CEP170 (Fig. 5 B), a key component of the centrosome that functions as a microtubule-organizing center, essential for the perinuclear localization of Golgi membranes (Rios and Bornens, 2003). Hence, we hypothesize that CCDC151 is a bridging factor between the centrosome and Golgi membranes via interactions with Golgin A5 and CEP170, thereby contributing to the maintenance of Golgi architecture. Disruption of this functional link after depletion of CCDC151 may result in Golgi membrane dispersion throughout the cytoplasm. Of interest, our results also revealed the presence of TTC17 and CCDC157 on Golgi

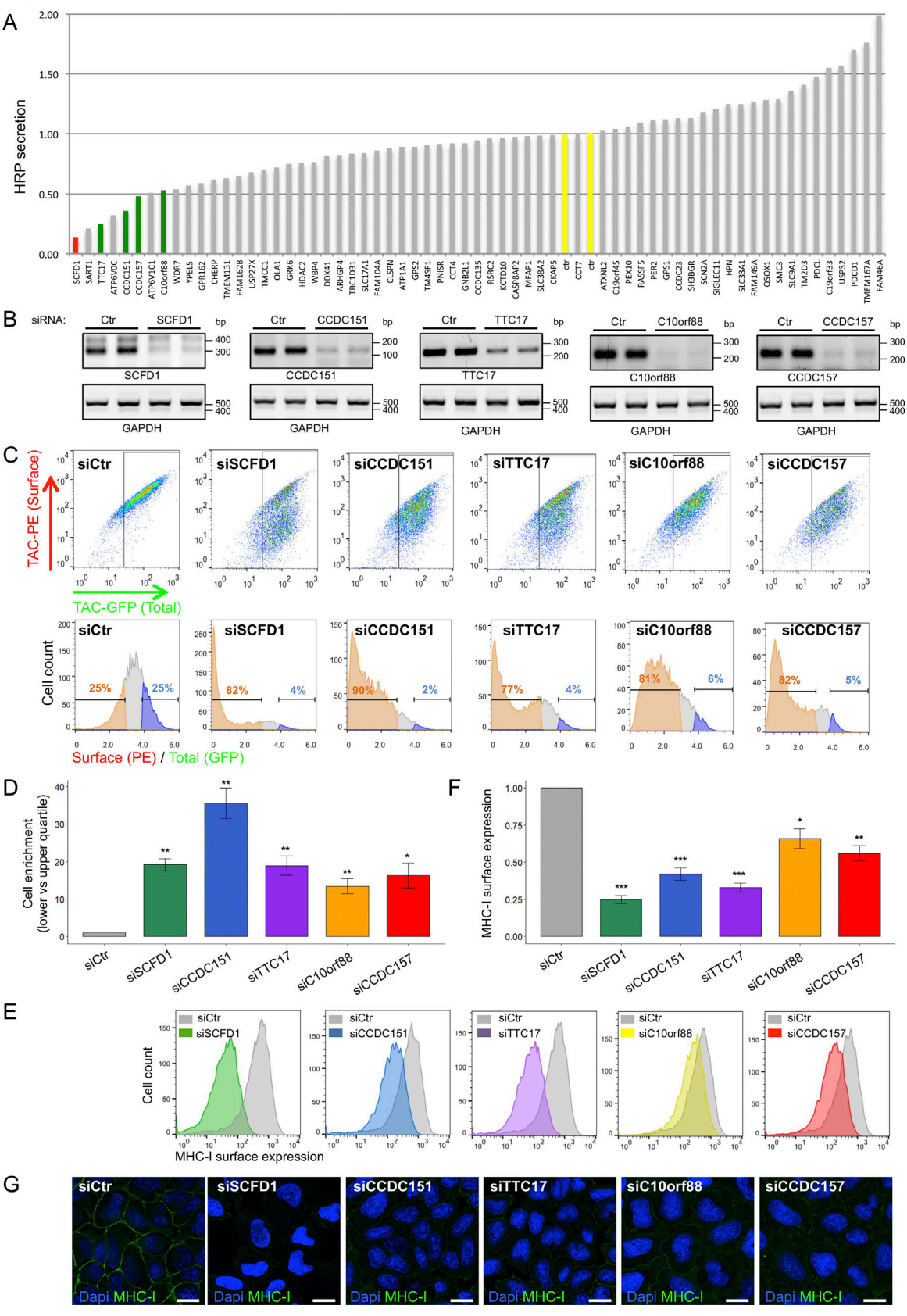

Figure 3. **Identification of new factors for protein transport and secretion. (A)** 62 genes with unknown or poorly characterized function that were identified as candidate genes either in the lower (39 genes) or upper quartiles (23 genes) were selected for a secondary screen using a secretion assay based on the detection of ss-HRP. HeLa–ss-HRP cells were plated in a 96-well plate prearrayed with specific smart pool siRNAs. After 3 d, cells were washed and

incubated for 8 h with complete medium. HRP secretion was monitored from the supernatant by chemiluminescence and normalized to internal HRP activity (n = 2). HRP quantification from cells transfected with control siRNA (in yellow) and siRNA targeting SCFD1 (in red) was used as negative and positive controls, respectively. Genes selected for further analysis are highlighted in green. Entire data are reported in Table S2. **(B)** HeLa TAC-GFP cells were transfected with the indicated specific individual siRNA and, after 3 d, knockdown efficiency of targeted genes was monitored by RT-PCR. **(C)** HeLa TAC-GFP cells were transfected with the indicated specific individual siRNA and after 3 d, surface and total TAC expressions (top panels) and surface/total TAC expression ratio (bottom panels) were analyzed by flow cytometry in living cells. In the bottom panels, lower and upper quartiles are set on control cells and applied to the other experimental conditions. **(D)** Quantification of the enrichment of cells in the lower quartile compared with the upper quartile as presented in C, bottom panels (mean of n = 4 ± SEM; two-tailed Student's t test for comparison to control condition siCtr; *, P < 0.05; **, P < 0.01). **(E and G)** HeLa cells were transfected with the indicated specific individual siRNA and after 3 d, surface MHC-I expression was analyzed on cells fixed with PFA without cell permeabilization by flow cytometry (E) and immunofluorescence microscopy (G; nuclei were stained with DAPI). Scale bars, 20 µm. **(F)** Quantification of the mean of fluorescence of MHC-I surface expression presented in E. Values were normalized to control sample (mean of n = 4 ± SEM; two-tailed Student's t test for comparison to control condition siCtr; *, P, < 0.05; **, P < 0.01; ***, P < 0.001).

membranes (Fig. 5, F, G, and I). A residual signal of C10orf88 was mainly diffuse in the cytoplasm (Fig. 5, H and I). The subcellular location of TTC17 and CCDC157, and the consequence of their knockdown on Golgi membranes, prompted us to further characterize these two factors.

CCDC157 is required for fusion events with Golgi membranes

A permanent flux of membrane traffics to and from the Golgi complex. BFA has been regularly used to study Golgi membrane dynamics, inducing a complete fusion of Golgi membranes with the ER and endosomes via tubule formation (Lippincott-Schwartz et al., 1989) and the relocation of peripheral matrix Golgi proteins such as GM130 and GRASP65 to the ER exit site (Mardones et al., 2006). First, we tested whether Golgi membrane reorganization was altered upon BFA treatment in TTC17- and CCDC157-depleted cells. HeLa cells were transfected with specific individual siRNAs and, after 3 d, treated with BFA. Immunofluorescence microscopy revealed that GM130 completely dispersed upon 30 min of BFA treatment in control cells and in most of the CCDC157- and TTC17-depleted cells (Fig. 6, A and B). Next, we tested the effects of CCDC157 and TTC17 knockdown on Golgi membrane reassembly after BFA washout, which is mediated by fusion events. In control and TTC17-depleted cells, Golgi membrane reassembly occurred in most cells after 60 min, while in CCDC157-depleted cells, GM130 remained completely dispersed (Fig. 6, A and B). Given these results demonstrating that Golgi membrane reassembly after BFA washout was strongly altered upon CCDC157 knockdown, we assessed the distribution of the ER-Golgi intermediate compartment (ERGIC) by immunofluorescence microscopy using an anti-ERGIC53 antibody. ERGIC is a collection of tubulovesicular membrane clusters that allow delivery of secretory cargo from ER exit sites to the Golgi complex in a COPII vesicle-dependent manner via homotypic and heterotypic fusion events (Lorente-Rodríguez and Barlowe, 2011). In control and TTC17-depleted cells, ERGIC53 staining mainly localized in the proximity of Golgi membranes, whereas in CCDC157-depleted cells, ERGIC53 staining was more dispersed throughout the cytoplasm (Fig. 6, C and D). These results suggested that CCDC157 could act as an important factor for the fusion of transport carriers with the Golgi complex.

To further test a role in membrane fusion, we assessed the impact of CCDC157 knockdown on the distribution of transport carriers derived from the endocytic pathway that fuse with Golgi membranes (Johannes and Popoff, 2008). We performed immunofluorescence microscopy experiments using an antibody targeting the transferrin (Tf) receptor (TfR), which, although it is mainly recycled to the plasma membrane after endocytosis (Huebers and Finch, 1987), is also retrieved to Golgi membranes (Snider and Rogers, 1985; Woods et al., 1986; Jin and Snider, 1993), and an antibody targeting EEA1, a marker of early endosomes, critical for endosomal trafficking (Barysch et al., 2009). We hypothesized that while TfR-containing transport carriers do not mainly fuse with Golgi membranes (Snider and Rogers, 1985; Woods et al., 1986), alteration of these fusion events could lead over time to the accumulation of transport carriers in the vicinity of the Golgi apparatus. In TTC17-depleted cells, the distribution of TfR and EEA1 was not markedly affected compared with control cells (Fig. 6, E and F; and Fig. S3). However, in CCDC157-depleted cells, the distribution of both TfR and EEA1 was strongly altered, most of the signal being coalesced to the perinuclear area in the form of enlarged TfR- and EEA1-positive vesicles, surrounded by Golgi membranes (Fig. 6, E–H; and Fig. S3). In line with these observations, the uptake as well as the recycling of Tf were reduced upon CCDC157 knockdown (Fig. S4). Altogether, these results suggested that in the absence of CCDC157, incoming carriers deriving from the endocytic pathway accumulated and coalesced in close proximity to Golgi membranes, strengthening CCDC157 as being an important factor for the fusion of transport carriers with the Golgi complex.

TTC17 is required for the polarized arrangement of Golgi cisternae and posttranslational modifications

In addition to being a gate entrance and a major sorting station, the Golgi apparatus allows posttranslational modifications such as glycosylation. This process is spatially regulated, being dependent on accurate localization of specific enzymes acting sequentially from the cis- to trans-Golgi cisternae. Does altered Golgi membrane organization in CCDC157- and TTC17-depleted cells impact Golgi polarization and create glycosylation defects? To address these questions, we first assessed the localization of GM130 and TGN46, cis- and trans-Golgi markers, respectively, in cells incubated in the presence or absence of nocodazole. Nocodazole is a microtubule-depolymerizing agent that causes Golgi ribbon dissociation and hence Golgi stack dispersion (Cole et al., 1996), facilitating the visualization of Golgi-resident protein segregation in individual Golgi stacks (Fig. 7, A and D). In

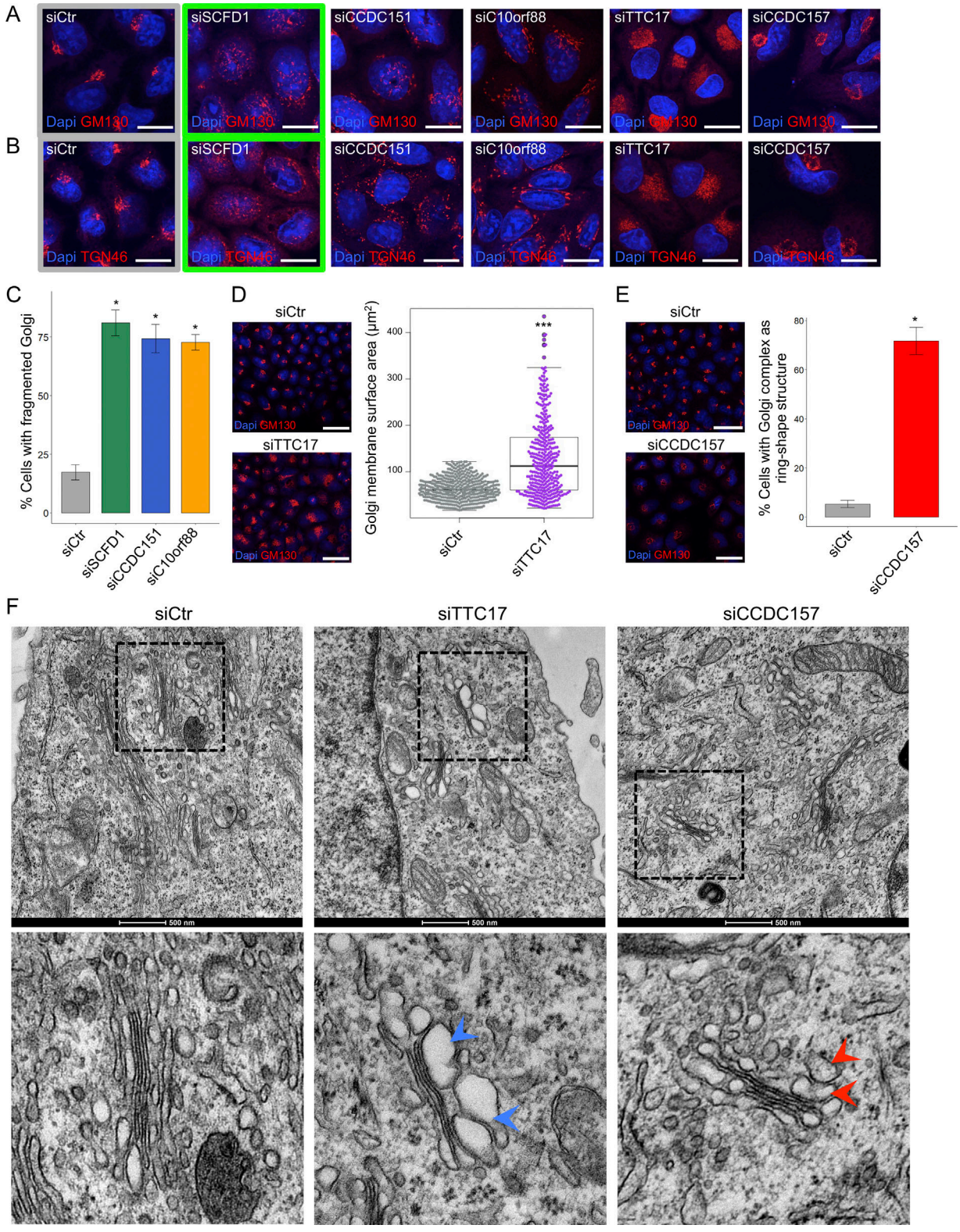

Figure 4. **Newly identified factors are essential for secretory pathway organization. (A and B)** HeLa cells were transfected with indicated specific individual siRNAs and after 3 d, analyzed by immunofluorescence microscopy using antibodies against GM130 (A) and TGN46 (B), respectively. Nuclei were stained with DAPI. Scale bars, 20 µm. **(C)** Quantification of the percentage of cells with fragmented Golgi complex after transfection with the indicated specific individual siRNAs. For unbiased analysis of Golgi membrane morphology, the classifier of the CellProfiler Analyst was used (see Materials and methods). At least 200 cells were analyzed for each independent experiment (mean of $n = 3 \pm$ SEM; two-tailed Student's t test for comparison to control condition siCtr; *, $P < 0.05$). **(D and E)** Left: HeLa cells were transfected with indicated specific individual siRNAs and after 3 d, analyzed by immunofluorescence microscopy using an anti-GM130 antibody. Nuclei were stained with DAPI. Scale bars, 50 µm. Right panel in D shows the quantification of Golgi surface area. For unbiased analysis

of Golgi membrane surface area, cells (465 control cells and 388 TTC17-depleted cells) were analyzed with the CellProfiler Analyst (See Materials and methods). Mann–Whitney *U* test for comparison to control condition siCtr; ***, P < 0.001. Right panel in E shows the quantification of the percentage of cells with Golgi membranes with a ring-shape structure using the classifier of the CellProfiler Analyst (See Materials and methods). At least 200 cells were analyzed for each independent experiment (mean of $n = 3 \pm$ SEM; two-tailed Student's *t* test for comparison to control condition siCtr; *, P < 0.05). **(F)** Transmission electron microscopy of Golgi membranes in control cells and TTC17- and CCDC157-depleted cells. Scale bars, 500 nm. In a given cell with altered Golgi membranes, all individual Golgi stacks had altered ultrastructure characterized by enlarged and swollen Golgi cisternae (blue arrowheads) in TTC17-depleted cells, and most likely accumulated and coalesced transport carriers in close proximity to Golgi membranes (red arrowheads) in CCDC157-depleted cells, respectively.

control cells, GM130 and TGN46 staining only partially colocalized (Pearson's correlation coefficient r = 0.507). Similar results were obtained in CCDC157-depleted cells (r = 0.495). Conversely, in TTC17-depleted cells, GM130 and TGN46 staining showed a high degree of colocalization (r = 0.805; Fig. 7, A–D), suggesting that protein localization in their respective cisternae was perturbed with no further segregation of cis- and trans-Golgi markers. In addition, we observed that upon TTC17 knockdown, nocodazole failed to induce complete Golgi membrane fragmentation, although the microtubule cytoskeleton was entirely depolymerized (Fig. 7 C). We hypothesized that the dramatic alteration of Golgi membrane architecture upon TTC17 depletion prevents efficient Golgi stack dissociation.

We next tested whether the loss of Golgi polarization in TTC17-depleted cells impairs cargo protein glycosylation. The lysosomal protein LAMP2 is highly glycosylated during its transport across the secretory pathway, increasing its molecular weight (Stewart et al., 2017). In control and CCDC157-depleted cells, immunoblotting analysis revealed LAMP2 mainly as a fully processed 100-kD band. However, in TTC17-depleted cells, a smaller form of ∼80 kD became apparent, indicating incomplete LAMP2 processing, likely related to a glycosylation defect (Fig. 7 E). These results established TTC17 as an important factor for Golgi membrane structure and polarized arrangement of Golgi cisternae, enabling cargo protein processing and transport.

Discussion

Although a large number of gene products involved in protein transport was identified in recent decades (Novick et al., 1980; Braell et al., 1984; Bard et al., 2006; Wendler et al., 2010), the list is far from complete, and several crucial issues are emerging. Indeed, in eukaryotic cells, evolution has given rise to an incredible diversity and complexity of cargo molecules, whose efficient and accurate transport along the secretory pathway is of paramount importance for organismal development, cell and tissue homeostasis, immunity, metabolic regulation, nerve transmission, and healthy aging (Rothman and Orci, 1992; Söllner and Rothman, 1994; Lee et al., 2004; Zanetti et al., 2012; Guo et al., 2014; Malhotra and Erlmann, 2015). An increasing number of studies has demonstrated that cells are endowed with specific structural and functional machinery that can be tightly regulated to cope with the whole spectrum of cargo proteins (Cancino et al., 2014; Ma et al., 2018; Raote et al., 2018; Lopes-da-Silva et al., 2019). In this context, it is essential to develop versatile and high-throughput screening strategies to uncover how secretory pathways are adapted to and are regulated in response to intrinsic demands and environmental cues, and altered in diseases.

In this study, we implemented an unbiased pooled genome-wide CRISPRi screen allowing us to efficiently identify new components of the secretory pathway. Major benefits have already been associated with pooled CRISPR screens, establishing such approaches as powerful tools for systematically defining gene function in mammalian cells (Gilbert et al., 2014; Shalem et al., 2015; Canver et al., 2018). The efficiency of our strategy relies on the combination of key parameters. First, we used a complementary reporter system associated with cell selection based on the ratio of two fluorescent signals. This reporter system allowed monitoring surface/total TAC expression ratio variations and therefore differential FACS-based cell sorting, directly relative to the transport of TAC protein to the cell surface. The strengths of this strategy were exemplified with Sec61A knockdown, where we could avoid following up undesirable phenotypes such as defective TAC protein synthesis. Second, as the secretory pathway is of critical importance for cell homeostasis and viability, gene expression was systematically down-regulated using the dCas9 fused to a KRAB effector domain for CRISPRi, instead of the active Cas9 for CRISPR knockout (Shalem et al., 2015; Kampmann, 2018). The resulting transcriptional repression of target genes preserved minimal gene expression, preventing massive cell death after down-regulation of key factors for protein and membrane trafficking. Third, the combination of the dual fluorescent reporter with the CRISPRi system allowed us to monitor TAC transport and perform FACS-based cell sorting at a relatively early time point (7 d after lentivirus transduction), which also would reduce excessive cell death after gene knockdown. Altogether, combining these technical parameters makes our approach a noteworthy advance compared with previous RNA interference–based genome-wide screens and resulted in a powerful platform allowing us to focus on the identification of genes involved in secretory pathway function and organization.

Our work highlighted several factors whose knockdown inhibited or promoted the trafficking of both exogenous and endogenous cargo proteins. Various genes encoding proteins known to be involved in calcium homeostasis, signaling pathways, or lysosomal activity, among others (Table S2), strengthen the idea that there are functional links between these cellular processes and the secretory pathway. In addition, several proteins with unknown or poorly characterized function were identified. In particular, TMEM167A, FAM46A, and USP32, which promote secretion upon knockdown, as well as C10orf88, WDR7, YPEL5, TMEM161, FAM162B, and GPR162, which inhibit secretion upon knockdown, deserve greater attention. For

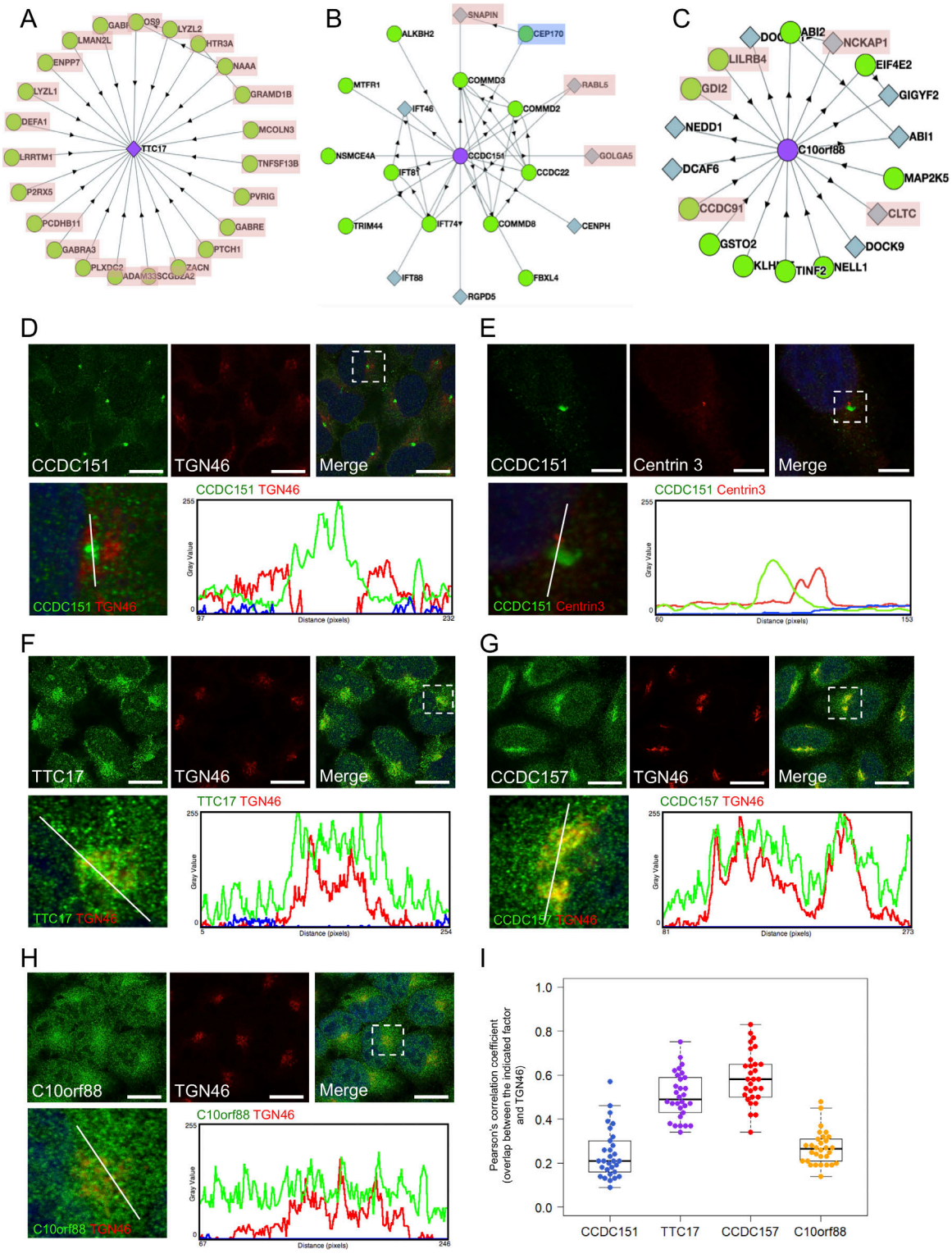

Figure 5. **Newly identified factors localize along the secretory pathway. (A–C)** BioPlex 2.0 analysis displaying interacting partners of TTC17 (A), CCDC151 (B), and C10orf88 (C). Functional proteins acting along the secretory pathway or cargo proteins transported along the ER-Golgi apparatus are highlighted in red. **(D–H)** HeLa cells were processed for cytosolic washout. Then, the colocalization of CCDC151 (D and E), TTC17 (F), CCDC157 (G), and C10orf88 (H; green) with TGN46 or centrin 3 (red) was assessed by immunofluorescence microscopy. Nuclei were stained with DAPI. Scale bars, 20 µm in D and F–H. Scale bars, 8 µm in E. Intensity profile graphs showing the relative localization of the indicated proteins were obtained along the lines shown in the confocal micrograph inserts. **(I)** Pearson's correlation coefficient of colocalization for the indicated proteins (r) derived from confocal micrographs (n = 30).

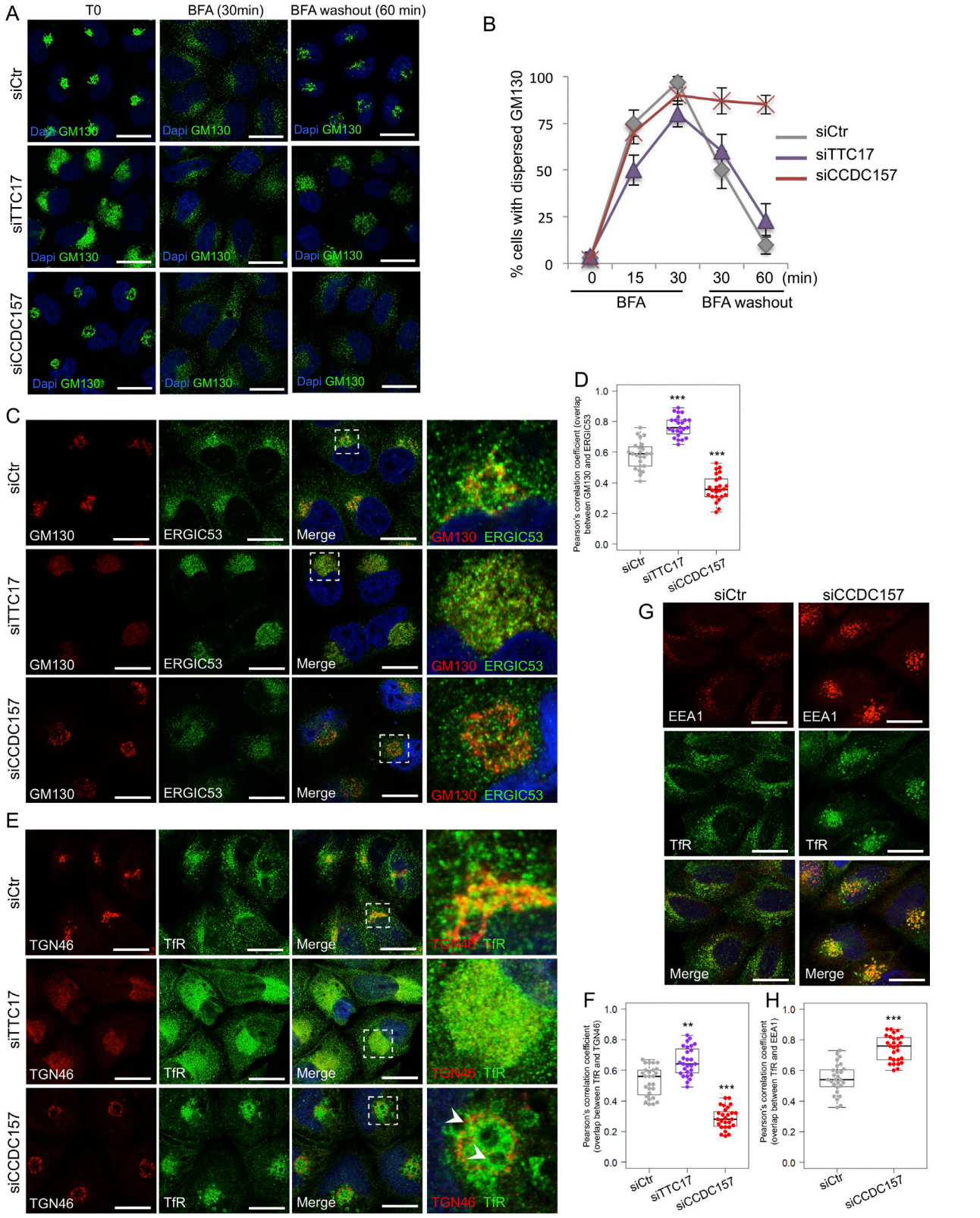

Figure 6. **CCDC157 is required for fusion events with Golgi membranes. (A)** Control HeLa cells and cells depleted of TTC17 or CCDC157 were incubated with 5 µg/ml BFA for the indicated times, after which cells were analyzed by immunofluorescence microscopy using an anti-GM130 antibody. For BFA washout, cells were incubated with BFA for 30 min, washed extensively, and incubated in BFA-free medium before immunofluorescence microscopy analysis. Nuclei were stained with DAPI. Scale bars, 20 µm. **(B)** Quantification of cells with dispersed Golgi membranes using an anti-GM130 antibody as described in A. 200 cells were counted per condition for each individual experiment (mean of $n = 3 \pm$ SEM). **(C)** Control HeLa cells and cells depleted of CCDC157 or TTC17 were analyzed by immunofluorescence microscopy using anti-ERGIC and anti-GM130 antibodies. Nuclei were stained with DAPI. Scale bars, 10 µm. **(D)** Pearson's

correlation coefficient of colocalization between ERGIC53 and GM130 (n = 24; Two-tailed Student's t test for comparison to control condition siCtr; ***, P < 0.001). **(E)** Control HeLa cells and cells depleted of CCDC157 or TTC17 were analyzed by immunofluorescence microscopy using anti-TfR and anti-TGN46 antibodies. Nuclei were stained with DAPI. Scale bars, 10 µm. Arrowheads point at enlarged and coalesced TfR-positive vesicles, surrounded by Golgi membranes. **(F)** Pearson's correlation coefficient of colocalization between TfR and TGN46 (n = 27; two-tailed Student's t test for comparison to control condition siCtr; **, P < 0.01; ***, P < 0.001). **(G)** Control HeLa cells and cells depleted of CCDC157 were analyzed by immunofluorescence microscopy using anti-EEA1 and anti-TfR antibodies. Nuclei were stained with DAPI. Scale bars, 10 µm. **(H)** Pearson's correlation coefficient of colocalization between EEA1 and TfR (n = 27; two-tailed Student's t test for comparison to control condition siCtr; ***, P < 0.001).

example, USP32 is a membrane-bound ubiquitin protease localized in the Golgi apparatus and overexpressed in breast cancer (Akhavantabasi et al., 2010); and GPR162 is an orphan GPCR. Compelling evidence suggests that the activation of GPCRs on Golgi membranes is critical for protein and membrane trafficking, but their identities remain elusive (Díaz Añel and Malhotra, 2005; Cancino et al., 2014; Eichel and von Zastrow, 2018). Altogether, our results provide a valuable resource to gain future important insights into fundamental mechanisms governing protein and membrane transport.

Our study further characterized two of the newly identified factors, TTC17 and CCDC157, as new actors of critical importance for the structure and function of Golgi membranes. Although additional studies will be required to fully decipher their roles, our results suggest that like other coiled-coil proteins (Wong and Munro, 2014; Cheung and Pfeffer, 2016) CCDC157 could be part of a tethering complex required for fusion events at the Golgi membranes. Furthermore, phenotypes observed in TTC17-depleted cells associated with TTC17 interacting partners involved in sphingomyelin metabolism (ENPP7 and NAAA; Fig. 5 A; Duan et al., 2003; Tsuboi et al., 2007) suggest that TTC17 could play a role in lipid production and distribution, critical parameters for Golgi membrane organization (van Galen et al., 2014; Campelo et al., 2017). Deciphering how CCDC157 and TTC17 are recruited to membranes and how their functions are coordinated with other structural factors and components of the tethering and fusion machinery will be of major interest.

In conclusion, while initial screens performed in yeast revealed the basic principles conserved across species (Novick et al., 1980), and, more recently, arrayed RNA interference screens revealed key players that function in metazoans (Bard et al., 2006; Saito et al., 2009; von Blume et al., 2009), our pooled CRISPRi screen unveiled new components that further refine the steps along the secretory pathway. In addition, we anticipate that the adaptation of our screening platform to specific cargo proteins, professional secretory cell types, and intrinsic or environmental challenges will open new and stimulating perspectives for a better understanding of the secretory pathway architecture in health and disease, for both conventional and unconventional secretion (Zhang and Schekman, 2013; Cruz-Garcia et al., 2018; Villeneuve et al., 2018; Chiritoiu et al., 2019).

Materials and methods

Antibodies, reagents, and plasmids

Antibodies used in this study included mouse monoclonal antibodies anti-TAC conjugated to PE (BioLegend; 356103), anti-GM130 (BD Biosciences; 610822), anti-Sec31A (BD Biosciences; 612351), anti–MHC-I (Thermo Fisher Scientific; MA1-70111), anti-EEA1 (BD Biosciences; 610457), anti–α-tubulin (Thermo Fisher Scientific; 62204), anti-LAMP2 (BioLegend; 354302) and anti-centrin3 (Novus Biologicals; H00001070-M01), a mouse polyclonal antibody anti-C10orf88 (Abcam; ab169106), a sheep polyclonal antibody anti-TGN46 (BioRad; AHP500), a rabbit monoclonal antibody anti-ERGIC53 (Abcam; ab125006), rabbit polyclonal antibodies anti-CNX (Abcam; ab22595), anti-CCDC151 (Abcam; ab151469), anti-TTC17 (Atlas Antibodies; HPA038508), anti-CCDC157 (GeneTex; GTX45090), anti-TfR (Abcam; ab84036); secondary antibodies donkey anti-sheep IgG–Alexa Fluor 568 (A21099), goat anti-mouse IgG–Alexa Fluor 488 (A11001), goat anti-mouse IgG–Alexa Fluor 568 (A11004), goat anti-rabbit IgG–Alexa Fluor 568 (A11011), and goat anti-rabbit IgG–Alexa Fluor 488 (A11034; Thermo Fisher Scientific); and a secondary antibody mouse IgGκ conjugated to HRP (Santa Cruz Biotechnology; sc-516102).

Reagents used in this study were obtained from the following sources: Dulbecco's PBS (D8662), BFA (B6542), nocodazole (M1404), puromycin (P9620), G-418 (4727878001), protease inhibitor cocktail (05892953001), trypsin (T3924), penicillin/streptomycin (P0781), and L-glutamine (G7513) were from Sigma-Aldrich. Q5 HF DNA polymerase (M0491L), Phusion HF DNA polymerase (M0530L), Phusion HF reaction Buffer (B0518S), and dNTPs (N0447S) were from New England Biolabs. T4 DNA ligase (EL0011), FBS (10270-106), Lipofectamine 2000 transfection reagent (12566014), DH5α bacteria (18258012), Restore Plus reagent (46430), ProLong Gold antifade reagent with DAPI (P36935), OptiMEM (319885062), and Tf conjugated with Alexa Fluor 647 (T23366) were from Thermo Fisher Scientific. TransIT-2020 transfection reagent (5405) and TransIT-293 transfection reagent (MIR2700) were from Mirus. Polybrene (TR-1003-G) and digitonin (11024-24-1) were from Merck. 0.45 µm low protein binding membrane (28145-479) was from VWR International. NucleoSpin Blood L kit (740569.10) was from Macherey-Nagel. ECL Western Blotting Detection Reagent (RPN2106) was from GE Healthcare. DMEM (D6546) was from Molecular Probes. SPRI AMPure XL beads were from Beckman Coulter. White CulturPlate 96-well plates (6005680) were from PerkinElmer. RNAeasy Plus Mini kit (74134) was from QIAGEN. Cloned AMV First-Strand cDNA Synthesis kit (12328032) was from Invitrogen. Mouse IgGκ Isotype (400111) was from BioLegend. Universal mycoplasma detection kit (30-1012K) was from American Type Culture Collection (ATCC).

Plasmids included pCMV6-AC-IL2R-GFP (Origene plasmid RG215768). pHR-SFFV-dCas9-BFP-KRAB was a gift from S. Qi (Stanford University, Stanford, CA) and J. Weissman (University of California, San Francisco, San Francisco, CA; Addgene plasmid 46911; Gilbert et al., 2013). pU6-sgRNA EF1Alpha-puro-T2A-BFP was a gift from J. Weissman (Addgene plasmid 60955; Gilbert

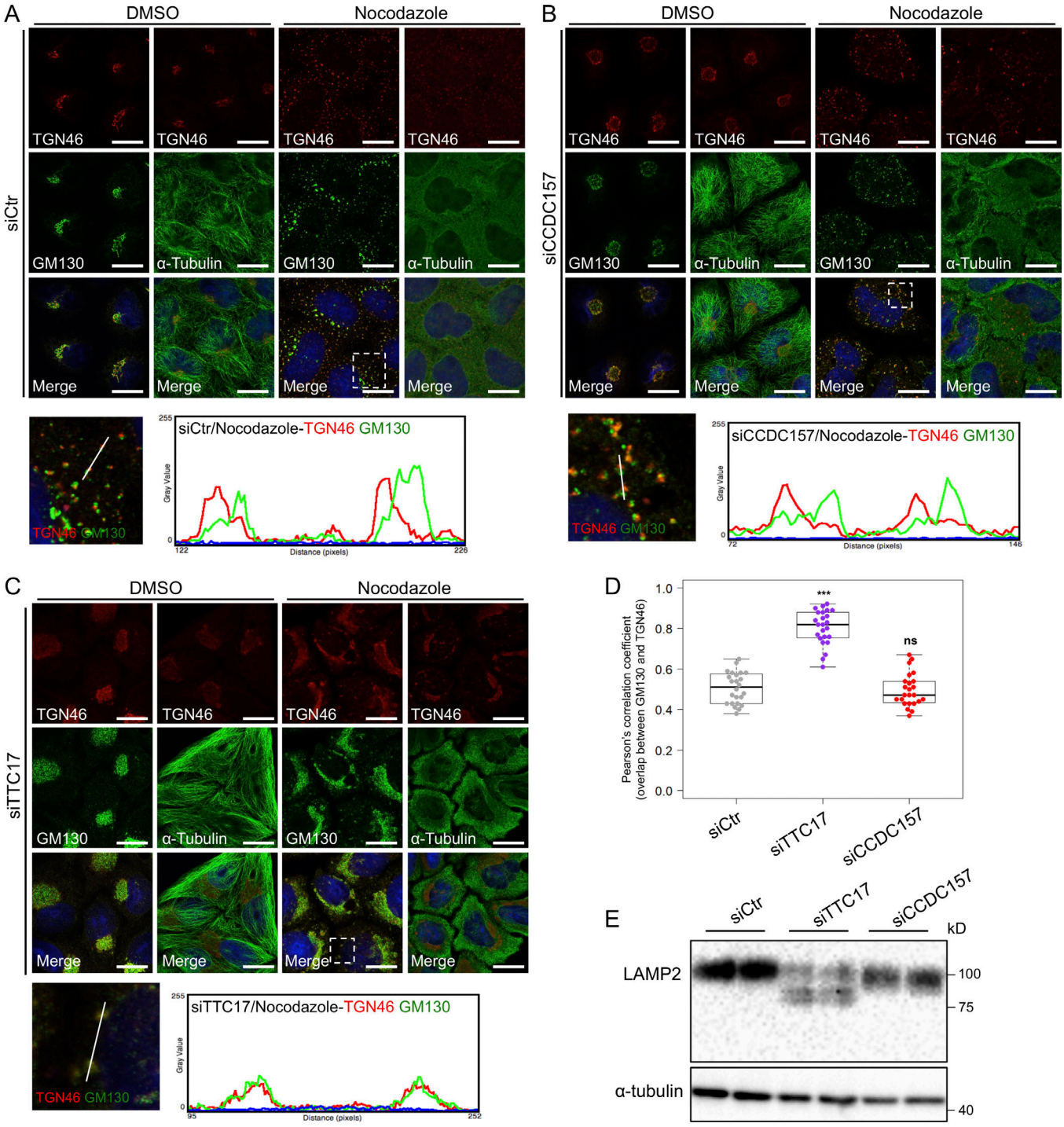

Figure 7. **TTC17 is required for the polarized arrangement of Golgi cisternae and posttranslational modifications. (A–C)** Control HeLa cells (A) and cells depleted of CCDC157 (B) or TTC17 (C) were incubated in the presence or absence (DMSO) of 500 ng/ml nocodazole for 2 h, and analyzed by immunofluorescence microscopy with anti-TGN46 and anti-GM130 antibodies. Depolymerization of the microtubule cytoskeleton was monitored with an anti–α-tubulin antibody. Nuclei were stained with DAPI. Scale bars, 10 µm. Insets from A, B, and C, show Golgi stack dispersion after nocodazole treatment. Intensity profile graphs of TGN46 and GM130 colocalization derived along the lines indicated in the confocal micrograph inserts. **(D)** Pearson's correlation coefficient of colocalization between TGN46 and GM130 from confocal micrographs acquired for control cells, and cells depleted of CCDC157 or TTC17 after nocodazole treatment (n = 24; two-tailed Student's t test for comparison to control condition siCtr; ***, $P < 0.001$; ns, statistically nonsignificant). **(E)** Total cell lysates of control HeLa cells and cells depleted of TTC17 or CCDC157 were analyzed by immunoblotting with anti-LAMP2 and anti–α-tubulin antibodies. Results are representative of three independent experiments.

et al., 2014). pCMV-VSV-G was a gift from B. Weinberg (Whitehead Institute for Biomedical Research, Cambridge, MA; Addgene plasmid 8454; Stewart et al., 2003). psPAX2 was a gift from D. Trono (École polytechnique fédérale de Lausanne, Lausanne, Switzerland; Addgene plasmid 12260). hCRISPRi-v2 genome-wide library was a gift from J. Weissman (Addgene pooled library 83969; Horlbeck et al., 2016a).

Cell culture

All cell lines, HeLa cells (ATCC), HeLa–ss-HPR cells (a gift from V. Malhotra, Centre for Genomic Regulation, Barcelona, Spain), HeLa TAC-GFP cells (this paper), HeLa TAC-GFP dCas9-KRAB cells (this paper), and HEK293T cells (ATCC) were grown in complete medium consisting of DMEM (Molecular Probes; D6546) containing 10% FBS (Thermo Fisher Scientific; 10270-106), 100 U/ml penicillin, 100 µg/ml streptomycin (Sigma-Aldrich; P0781), and 2 mM L-glutamine (Sigma-Aldrich; G7513) at 37°C with 5% CO_2. All cell lines were tested every month using ATCC universal mycoplasma detection kit (ATCC; 30-1012K) to confirm they were clear of contamination by mycoplasma.

To generate a HeLa cell line stably expressing GFP-tagged TAC protein, we transfected HeLa cells with pCMV6-AC-IL2R-GFP (Origene; plasmid RG215768) using TransIT-2020 transfection reagent (Mirus; 5405), following the manufacturer's recommendations, and after 2 d, transfected cells were selected with 600 µg/ml G-418 (Sigma-Aldrich; 4727878001) during 1 wk. Then, GFP-positive cells were isolated by FACS, and single cells were collected in 96-well plates. After expansion into the 6-well format, TAC-GFP expression was assessed from clonal lines by flow cytometry and immunofluorescence microscopy analysis. The GFP signal allows monitoring the total TAC expression, whereas the pool expressed at the cell surface can be assessed using a PE-conjugated antibody, which recognizes the extracellular domain of the TAC protein. To generate HeLa TAC-GFP dCas9-KRAB cells, we transduced HeLa TAC-GFP cells with lentivirus to express dCas9-KRAB-BFP fusion protein (see section Lentivirus production and transduction). After 2 d, transduced cells were sorted for GFP- and BFP-positive cells.

siRNA-mediated knockdown

Specific individual siRNA and smart pools siRNA were transfected in HeLa cells, HeLa–ss-HPR cells, and HeLa TAC-GFP cells using Lipofectamine 2000 transfection reagent (Thermo Fisher Scientific; 12566014) following the manufacturer's recommendations. Individual siRNA and smart pools siRNA were purchased from Dharmacon. The siRNA sequences used were the following: control 5′-CGUACGCGGAAUACUUCGA-3′, SCFD1 5′-AGACUUAUUGAUCUCCAUA-3′, TTC17 5′-GAAUACGGGUGC UGAAGAA-3′, 5′-GGAGAGAGUUAAUCUUUCU-3′, 5′-GGACCU GGAUCUAUAUGAU-3′, 5′-GGACCAGCCUGUACGCUAU-3′, CCDC157 5′-GGAAAGACCUGACGCGCCU-3′, 5′-ACUACGGACCUGCGGCUAA-3′, 5′-CUGAGUGGGAGCACGACAA-3′, 5′-CAGCGUGGAAUCCCAGAU A-3′, CCDC151 5′-GCUCAAGGCCUAUCUAAUG-3′, 5′-GAAGGCUGC CCGAAUACAA-3′, 5′-CGGGAACGCUACAUAAGUG-3′, 5′-GCACAU UACCAGCGUGUAC-3′, and C10orf88 5′-GCACAUUGAUGAUAAGAU U-3′, 5′-GAAAUAAGACCGAGUGUCA-3′, 5′-GCUCAGCAGUUGAUG GAUA-3′, 5′-GGGAUACCUCUAAGACAUU-3′. After incubation for 72 h, total RNA was extracted and knockdown efficiency was assessed by RT-PCR.

CRISPRi-mediated knockdown

Gene-specific CRISPRi sgRNA oligonucleotide sequences used were the following: Gal4 5′-GAACGACTAGTTAGGCGTGTA-3′, Sec61A 5′-GGCTAGCACTGACGTGTCTCT-3′, SCFD1 5′-GAGCAG CCAGTATTCGGGAA-3′, and Sec24A 5′-GACATGATGACTGGG TTGGA-3′. Forward sgRNA oligonucleotides were designed with 5′-TTG and 3′-GTTTAAGAGC overhangs, and reverse sgRNA oligonucleotides were designed with 5′-TTAGCTCTTAAAC and 3′-CAACAAG overhangs. Oligonucleotides were diluted to 100 µM in water, and 1 µl of forward and reverse oligo was combined in a 50-µl reaction containing 200 mM potassium acetate, 60 mM Hepes, pH 7.4, and 4 mM magnesium acetate. Oligonucleotides were incubated for 5 min at 95°C and slow-cooled (0.1°/s) for annealing. Annealed oligos were diluted 1/40, and 1 µl of insert was ligated into 10 ng of digested vector (pU6-sgRNA EF1Alpha-puro-T2A-BFP; Addgene; plasmid 60955 digested with BstXI and Blpl) using T4 DNA ligase (Thermo Fisher Scientific; EL0011) in a final volume of 10 µl. Ligation was allowed to proceed for 1 h. Ligated products were transformed into DH5α bacteria (Thermo Fisher Scientific; 18258012). After lentivirus production (see section Lentivirus production and transduction), TAC-GFP-dCas9-KRAB HeLa cells were infected, and knockdown efficiency was monitored 7 d after transduction by RT-PCR. TAC-GFP expression was assessed by flow cytometry analysis.

Lentivirus production and transduction

Lentivirus was generated in HEK293T cells using TransIT-293 transfection reagent (Mirus; MIR2700) following the manufacturer's recommendations. At 50% confluence, HEK293T cells incubated in complete medium lacking penicillin/streptomycin were transiently transfected with a lentiviral vector, either pHR-SFFV-dCas9-BFP-KRAB (Addgene plasmid 46911) for dCas9-KRAB fusion protein expression, pU6-sgRNA EF1Alpha-puro-T2A-BFP (Addgene plasmid #0955) containing gene-specific CRISPRi sgRNA oligonucleotides, or hCRISPRi-v2 library (Addgene pooled library 83969) for a pooled genome-wide CRISPRi screen, together with packaging plasmids pCMV-VSV-G (Addgene plasmid 8454) and psPAX2 (Addgene plasmid 12260) at a 4:1:3 ratio. Transfection was performed using one 10-cm dish for dCas9-KRAB fusion protein expression and for each specific sgRNA, and using two 15-cm dishes for hCRISPRi-v2 library. After transfection (24 h), the medium was refreshed, and after an additional 24 h, virus was collected and filtered through a 0.45-µm low protein binding membrane (VWR International; 28145-479). For dCas9-KRAB fusion protein expression and CRISPRi-mediated knockdown, 1 ml of medium was used immediately for infection of ∼500,000 target cells plated in 6-well plate in a final volume of 2 ml. For a pooled genome-wide CRISPRi screen, ∼200 million TAC-GFP-dCas9-KRAB HeLa cells plated in thirty 15-cm dishes were infected at an MOI of 0.3. Medium was supplemented with 8 µg/ml polybrene (Merck; TR-1003-G) lacking penicillin/streptomycin.

After 24 h, medium was replaced with fresh medium, and after an additional 24 h, high BFP-positive cells expressing dCas9-KRAB fusion protein were sorted by FACS. For CRISPRi-mediated knockdown and a pooled genome-wide CRISPRi screen, 48 h after infection, 2 µg/ml puromycin (Sigma-Aldrich; P9620) was added to select transduced cells.

Pooled genome-wide CRISPRi screen and Illumina library construction and sequencing

Approximately 200 million HeLa cells stably expressing TAC-GFP and dCas9-KRAB fusion protein were transduced with the hCRISPRi-v2 library (Addgene; 83969) at an MOI of 0.3 to ensure no more than one viral integration event per cell. The CRISPi-v2 library comprised 104,535 sgRNAs targeting 18,905 human genes. Each sgRNA of the library targeted the TSS of the respective genes in regions of low nucleosome occupancy avoiding genomic DNA compaction to impact Cas9 binding (Horlbeck et al., 2016a,b). 2 d after infection, an aliquot of cells was analyzed by FACS to confirm transduction efficiency, and then cells were cultured with 2 µg/ml puromycin (Sigma-Aldrich) to remove uninfected cells. After five additional days, cells were trypsinized, washed extensively, and plated with fresh medium for 18 h, allowing recovery of transmembrane protein expression at the cell surface. Cells were then detached using 0.5 mM EDTA, resuspended in blocking buffer (OptiMEM containing 5% FBS), and stained for TAC surface expression using a PE-conjugated anti-TAC antibody during 1 h at 4°C. Finally, live cells were sorted by FACS following the PE/GFP fluorescence ratio, selecting the upper and lower quartile, respectively. 10 million cells were sorted for each fraction (Parnas et al., 2015; Park et al., 2017; Menzies et al., 2018). Cell sorting was performed using a FACSAria sorter. Two independent screens were performed. After FACS sorting, cells were centrifuged, and pellets were frozen until processing.

Genomic DNA was extracted from four distinct cell populations, corresponding to the upper and lower quartile of the PE/GFP fluorescence ratio, from two independent screens, using the NucleoSpin Blood L kit (Macherey-Nagel; 740569.10) according to the manufacturer's instructions. Then, for each sample, all genomic DNA was amplified by PCR to enrich sgRNA sequences. Each 100 µl PCR reaction contained 1× Phusion HF reaction Buffer (NEB; B0518S), 3% vol/vol DMSO, 0.4 µM of each forward and reverse primer mix (Integrated DNA Technologies), 0.2 mM dNTPs (NEB; N0447S), 40 U/ml Phusion HF DNA polymerase (NEB; M0530L), and 2 µg genomic DNA. PCR primer sequences for the forward primers with specific barcode for demultiplexing were the following: 5′-AATGATACGGCGACCACCGAGATCTACACGATCGGAAGAGCACACGTCTGAACTCCAGTCACCTTGTAGCACAAAAGGAAACTCACCCT-3′, 5′-AATGATACGGCGACCACCGAGATCTACACGATCGGAAGAGCACACGTCTGAACTCCAGTCACGCCAATGCACAAAAGGAAACTCACCCT-3′, 5′-AATGATACGGCGACCACCGAGATCTACACGATCGGAAGAGCACACGTCTGAACTCCAGTCACAGTTCCGCACAAAAGGAAACTCACCCT-3′, and 5′-AATGATACGGCGACCACCGAGATCTACACGATCGGAAGAGCACACGTCTGAACTCCAGTCACTAGCTTGCACAAAAGGAAACTCACCCT-3′, The PCR primer sequence for the common reverse primer was 5′-CAAGCAGAAGACGGCATACGAGATCGACTCGGTGCCACTTTTTC-3′. PCR cycling conditions used included 1× 98°C for 30 s, 23× 98°C for 30 s, 56°C for 15 s, 72°C for 15 s, and 1× 72°C for 10 min. For each sample, PCR products were pooled, size-selected using SPRI AMPure XL beads (Beckman Coulter) following the manufacturer's recommendations, and quantified on a Qubit and run on a Bioanalyzer (Agilent). The four libraries were pooled to a total concentration of 10 nM and subjected to DNA sequencing on a HiSeq2500 (Illumina) sequencer. Samples were sequenced with the rapid run mode of the single-ended 50 bp, following the manufacturer's recommendations, using a custom sequencing primer: 5′-GTGTGTTTTGAGACTATAAGTATCCCTTGGAGAACCACCTTGTTG-3′.

For data analysis, raw sequencing reads were aligned to the v2CRISPRi library sequences using Bowtie 2, and data were analyzed using the MAGeCK algorithm (Li et al., 2014). For genes with multiple independent TSS targeted by the sgRNA library, we calculated phenotype and P values independently for each TSS.

Secondary screen using an HRP secretion assay

As we intended to validate hit genes found in our primary screen with a secondary screen, hit genes were selected as interesting candidates among those with a P value <0.01 and a log2 fold change (lfc) less than −0.5 for genes enriched in the lower quartile and a lfc >0.3 for genes enriched in the upper quartile (see Tables S1 and S2). The difference of lfc cutoff applied for the selection of candidate genes relied on the weaker phenotypes observed on TAC transport for genes enriched in the upper quartile compared with those enriched in the lower quartile. Thus, 62 genes identified either in the lower (39 genes) or upper quartiles (23 genes) as candidate genes with an unknown or poorly characterized function were selected for a secondary screen using a secretion assay based on the detection of ss-HRP. HeLa cells stably expressing ss-HRP were transfected in a 96-well plate prearrayed with specific smart pools siRNA (Dharmacon) targeting selected genes, using Lipofectamine 2000 transfection reagent (Thermo Fisher Scientific; 12566014). Briefly, for each well, 3,000 HeLa–ss-HRP cells in 80 µl of complete medium lacking penicillin/streptomycin were plated into a 96-well plate containing 20 µl of 250 nM siRNA and 0.5% (vol/vol) Lipofectamine 2000 in OptiMEM (Thermo Fisher Scientific; 319885062). Medium was replaced after 24 h. After two additional days, cells were washed with medium and incubated with 150 µl of complete medium for 8 h. Then 50 µl of the medium was collected and mixed with ECL reagent (GE Healthcare; RPN2106) in white CulturPlate 96-well plates (PerkinElmer; 6005680), and the chemiluminescence was measured in a Tecan Microplate reader M1000 PRO. For normalization, cells were lysed with lysis buffer supplemented with protease inhibitors to quantify intracellular HRP activity.

Flow cytometry

After CRISPRi- or siRNA-mediated target gene knockdown, cells were washed with PBS and detached by incubation with 0.5 mM EDTA in PBS for 10 min. Cells were then resuspended in blocking buffer (OptiMEM containing 5% FBS), and live cells

were incubated for 1 h at 4°C with an anti-TAC antibody conjugated to PE. GFP and PE fluorescence were collected on a LSR Fortessa (BD Biosciences) and analyzed using FlowJo software (FlowJo). For surface MHC-I expression, cells were washed with PBS and detached by incubation with 0.5 mM EDTA in PBS for 10 min. Cells were then fixed with 4% (wt/vol) PFA in PBS for 15 min at room temperature, washed, and incubated for 1 h at 4°C with an anti–MHC-I antibody. The epitope recognized by the anti–MHC-I antibody localizes in the extracellular domain of MHC-I. Cells were washed again, incubated with a goat anti-mouse IgG–Alexa Fluor 488 and fluorescent signals collected on a LSR Fortessa (BD Biosciences) and analyzed using FlowJo software (FlowJo). For Tf internalization and recycling, see section FACS-based endocytosis and recycling assays.

FACS-based endocytosis and recycling assays

Control HeLa cells and cells knocked down for TTC17 and CCDC157 were detached with 0.5 mM EDTA for 10 min, washed in serum-free medium, and incubated at 4°C for 30 min in the presence of 50 µg/ml Tf conjugated with Alexa Fluor 647 (Thermo Fisher Scientific; T23366). Cells were then incubated at 37°C and at different type points (0, 2, 5, 10, and 15 min), Tf internalization was stopped by placing cells on ice for 10 min. Cells were then fixed with 4% (wt/vol) PFA in PBS for 15 min at room temperature and analyzed by flow cytometry on a LSR Fortessa (BD Biosciences). For recycling assay, cells were incubated with 50 µg/ml Tf conjugated with Alexa Fluor 647 for 30 min at 37°C, washed, and incubated at 37°C with 100 µg/ml unlabeled Tf for different time points (0, 5, 10, 15, and 30 min). Cells were then fixed with 4% PFA and analyzed by flow cytometry.

Immunoblot

Cells were lysed for 30 min on ice in lysis buffer (50 mM Tris, pH 7.4, 150 mM NaCl, 0.1% SDS, 1% (vol/vol) Triton X-100, and 0.5% sodium deoxycholate) supplemented with protease inhibitor cocktail (Sigma-Aldrich; 05892953001), 1 mM Na_3VO_4, and 25 mM sodium fluoride and centrifuged at 16,000 × *g* for 15 min. Samples were incubated with 1× SDS sample buffer at 95°C for 10 min, resolved by 12% SDS-PAGE, and transferred to methanol activated Immobilon-P 0.45 µm polyvinylidene difluoride membranes for blotting. Membranes were blocked with 5% (wt/vol) BSA in PBS containing 0.1% Tween 20 (PBS-T) for 30 min at room temperature and probed with appropriate primary antibodies overnight at 4°C in PBS-T containing 5% (wt/vol) BSA. Membranes were then washed 3 × 15 min in PBS-T and incubated with the corresponding HRP-conjugated secondary antibody for 1 h at room temperature in PBS-T containing 5% (wt/vol) BSA. Membranes were then washed again for 3 × 15 min in PBS-T, and signals were detected with ECL Western Blotting Detection Reagent (GE Healthcare; RPN2106) and acquired with the Chemidoc MP Imaging System (Bio-Rad). Membranes were stripped with Restore Plus (Thermo Fisher Scientific; 46430) according to the manufacturer's instructions.

Immunofluorescence microscopy

Cells grown on coverslips were fixed with cold methanol for 10 min at −20°C or 4% (wt/vol) PFA in PBS for 15 min at room temperature. Cells fixed with PFA were permeabilized with 0.1% Triton X-100 in PBS at room temperature and then incubated with blocking buffer (2.5% [wt/vol] FCS and 0.1% Triton X-100 in PBS) for 30 min at room temperature. Cells were then incubated with primary antibody diluted in blocking buffer for 1 h at room temperature followed by PBS wash and incubated with secondary antibody. Secondary antibodies conjugated with Alexa Fluor 488, 568, or 647 were diluted in blocking buffer and incubated 1 h at room temperature. Samples were mounted using ProLong Gold antifade reagent with DAPI (Thermo Fisher Scientific; P36935). Images were acquired with a Leica SP8 laser confocal scanning microscope with a 40× objective. Images displayed in figures are representative single Z-slices. After acquisition, images were processed using an Airyscan processing tool on the ZEN software provided by Zeiss.

For cytosol washout prior to immunofluorescence microscopy, cells were washed twice with room temperature KHM buffer (125 mM potassium acetate, 25 mM Hepes-KOH, pH 7.2, and 2.5 mM magnesium acetate). Cells were then permeabilized by incubation in KHM buffer containing 30 µg/ml digitonin for 5 min on ice followed by a wash for 5 min at room temperature with KHM buffer. Cells were subsequently fixed with 4% PFA and processed for immunofluorescence microscopy. This procedure allows the removal of soluble cytoplasmic pool of proteins, highlighting their potential association with intracellular compartments.

The level of colocalization was determined by acquiring confocal images from ∼30 cells per condition. Colocalization quantifications were performed using Coste's method of thresholding with object Pearson's analysis using Imaris 8.2.0 by Bitplane AG. Intensity profile graphs of the confocal images were calculated by a pixel-based method by ImageJ (National Institutes of Health).

For unbiased analysis of Golgi membrane surface area, images were analyzed with the CellProfiler software (Broad Institute; Dao et al., 2016). For each image analyzed, the area of Golgi membranes, identified as object, was extracted using the module "MeasureObjectSizeShape." For unbiased analysis of Golgi membrane morphology, the classifier of the CellProfiler Analyst was trained using cells randomly chosen from the whole experiment. These were classified as having a ring shape structure, fragmented, or intact Golgi. The classifier of the CellProfiler Analyst was then used to define, for all cells, Golgi membrane morphology on object level.

In all experiments, images shown in individual panels were acquired using identical exposure times and scan setting and adjusted identically for brightness and contrast using Photoshop CS5 (Adobe).

Transmission electron microscopy

3 d after transfection with individual specific siRNA, control HeLa cells and cells knocked down for TTC17 and CCDC157 were fixed with 2% PFA–2% glutaraldehyde solution in sodium cacodylate buffer for 1 h at room temperature. Cells were carefully detached using a plastic cell scraper, collected into Eppendorf tubes and centrifuged to obtain the pellet. Cells were then post-fixed for 30 min in 1% OsO4 at room temperature, washed three

times in distilled water and post-fixed for 1 h in 1% uranyl acetate. The pellets were dehydrated in graded steps of ethanol (50, 70, 90, 96, and 100%), two times in 100% of propylene oxide, and embedded into epon. Sections (60 nm thick) were cut on a Leica UC7 ultramicrotome and examined with a Fei Tecnai 12 BioTwin Spirit transmission electron microscope.

RT-PCR

Total RNA was extracted from HeLa cells using the RNAeasy Plus Mini kit (QIAGEN; 74134), and cDNAs were synthesized with the Cloned AMV First-Strand cDNA Synthesis kit (Invitrogen; 12328032) and oligo $d(T)_{20}$ according to the manufacturer's instruction. cDNA of indicated genes was amplified by PCR using Q5 HF DNA polymerase (NEB; M0491L) and the following specific primers: GAPDH forward primer 5′-ACCACC ATGGAGAAGGCTGG-3′, reverse primer 5′-CTCAGTGTAGCC CAGGATGC-3′, PCR product size: 527 bp; SCFD1 forward primer 5′-GGGGAAGATGAAGGAGCCATA-3′, reverse primer 5′-TCA GCCTCAGAAGGTGCTTG-3′, PCR product size: 319 bp; Sec24A forward primer 5′-CCATTGTCCTCGTGCATCAT-3′, reverse primer 5′-TGCCAATAAGCCACCTCCTT-3′, PCR product size: 369 bp; Sec61A forward primer 5′-AGTGGACCTGCCAATCAA GT-3′, reverse primer 5′-CTTTGGCAGAGGAACCTGAG-3′, PCR product size: 379 bp; TTC17 forward primer 5′-CAGATGACCATG CACGAAAAA-3′, reverse primer 5′-GTTGGCCAAGTTGACAAG AGG-3′, PCR product size: 248 bp; CCDC157 forward primer 5′-GCAGCCCACCCACTGTAATAA-3′, reverse primer 5′-TGCCCT GGGTGTACTCTCCTA-3′, PCR product size: 236 bp; C10orf88 forward primer 5′-TACACAACTGCCTGGTGGAGA-3′, reverse primer 5′-CGGTCTTATTTCCCACATGGA-3′, PCR product size: 218 bp; and CCDC151 forward primer 5′-TGAACCAAGAGGCCC TCAAT-3′, reverse primer 5′-GCGCTCGTTCTCCAGTTTCT-3′, PCR product size: 148 bp. The PCR products were resolved on 1.5% agarose gel.

Statistical analysis

The statistical details of all experiments are indicated in the figure legends, including statistical analysis performed, error bars, statistical significance, and experiment numbers (n). Statistics were performed using GraphPad Prism 6 software.

Online supplemental material

Fig. S1 shows the establishment of the cell line expressing a dual fluorescent reporter for protein transport based on the TAC-GFP expression, and the optimization of experimental conditions to assess TAC surface expression by flow cytometry. Fig. S2 shows the ER exit site and ER organization in control cells and in TTC17- and CCD157-depleted cells visualized by immunofluorescence microscopy. Fig. S3 shows the effect of TTC17 and CCDC157 knockdown on EEA1 distribution visualized by immunofluorescence microscopy. Fig. S4 shows the effect of TTC17 and CCDC157 knockdown on the uptake and recycling of Tf analyzed by flow cytometry. Table S1 shows MAGeCK analysis of the pooled genome-wide CRISPRi screen replicate. Table S2 shows the 62 candidate genes selected from the CRISPRi screen and results of the secondary screen using a secretion assay based on the detection of ss-HRP by chemiluminescence.

Acknowledgments

We thank members of the Moreau laboratory for helpful discussion.

S.J. Popa acknowledges support from a Wellcome Trust PhD studentship (109152/z/15/z). S.E. Stewart acknowledges support from a Biotechnology and Biological Sciences Research Council Future Leader Fellowship (BB/P010911/1). F. Campelo acknowledges financial support from the Spanish Ministry of Economy and Competitiveness ("Severo Ochoa" program for Centres of Excellence in R&D [SEV-2015-0522], FIS2015-63550-R, FIS2017-89560-R, and BFU2015-73288-JIN, AEI/FEDER/UE), Fundació Privada Cellex, and the Generalitat de Catalunya through the CERCA program. A. Ashok acknowledges support from a La Caixa Foundation fellowship. J. Villeneuve acknowledges support from a Marie Curie fellowship within the the European Union's Horizon 2020 research and innovation program (842919). D.C. Rubinsztein is grateful for support from the UK Dementia Research Institute (funded by the Medical Research Council, Alzheimer's Research UK, and the Alzheimer's Society) and the Roger de Spoelberch Foundation. This work was supported by a Wellcome Trust Strategic Award (100574/Z/12/Z), the Medical Research Council Metabolic Diseases Unit (MRC_MC_UU_12012/5), and the Isaac Newton Trust/Wellcome Trust Institutional Strategic Support Fund/University of Cambridge research grant.

The authors declare no competing financial interests.

Author contributions: J. Villeneuve, K. Moreau, V. Malhotra, R. Schekman, D.C. Rubinsztein, J. Weissman, and J. Ripoche conceptualized the experiments. J. Villeneuve and L. Bassaganyas performed and analyzed most of the experiments, with contributions from S.J. Popa, M. Horlbeck, C. Puri, S.E. Stewart, F. Campelo, A. Ashok, C.M. Butnaru, N. Brouwers, and K. Heydari. J. Villeneuve wrote the original and revised manuscripts with contribution from the other authors.

Submitted: 20 February 2019
Revised: 16 June 2019
Accepted: 12 August 2019

References

Akhavantabasi, S., H.B. Akman, A. Sapmaz, J. Keller, E.M. Petty, and A.E. Erson. 2010. USP32 is an active, membrane-bound ubiquitin protease overexpressed in breast cancers. *Mamm. Genome.* 21:388–397. https://doi.org/10.1007/s00335-010-9268-4

Asensio, C.S., D.W. Sirkis, and R.H. Edwards. 2010. RNAi screen identifies a role for adaptor protein AP-3 in sorting to the regulated secretory pathway. *J. Cell Biol.* 191:1173–1187. https://doi.org/10.1083/jcb.201006131

Bard, F., L. Casano, A. Mallabiabarrena, E. Wallace, K. Saito, H. Kitayama, G. Guizzunti, Y. Hu, F. Wendler, R. Dasgupta, et al. 2006. Functional genomics reveals genes involved in protein secretion and Golgi organization. *Nature.* 439:604–607. https://doi.org/10.1038/nature04377

Barysch, S.V., S. Aggarwal, R. Jahn, and S.O. Rizzoli. 2009. Sorting in early endosomes reveals connections to docking- and fusion-associated factors. *Proc. Natl. Acad. Sci. USA.* 106:9697–9702. https://doi.org/10.1073/pnas.0901444106

Braell, W.A., W.E. Balch, D.C. Dobbertin, and J.E. Rothman. 1984. The glycoprotein that is transported between successive compartments of the Golgi in a cell-free system resides in stacks of cisternae. *Cell.* 39:511–524. https://doi.org/10.1016/0092-8674(84)90458-6

Brandman, O., and R.S. Hegde. 2016. Ribosome-associated protein quality control. *Nat. Struct. Mol. Biol.* 23:7–15. https://doi.org/10.1038/nsmb.3147

Campelo, F., J. van Galen, G. Turacchio, S. Parashuraman, M.M. Kozlov, M.F. García-Parajo, and V. Malhotra. 2017. Sphingomyelin metabolism controls the shape and function of the Golgi cisternae. *eLife.* 6:e24603. https://doi.org/10.7554/eLife.24603

Cancino, J., A. Capalbo, A. Di Campli, M. Giannotta, R. Rizzo, J.E. Jung, R. Di Martino, M. Persico, P. Heinklein, M. Sallese, and A. Luini. 2014. Control systems of membrane transport at the interface between the endoplasmic reticulum and the Golgi. *Dev. Cell.* 30:280–294. https://doi.org/10.1016/j.devcel.2014.06.018

Canver, M.C., M. Haeussler, D.E. Bauer, S.H. Orkin, N.E. Sanjana, O. Shalem, G.C. Yuan, F. Zhang, J.P. Concordet, and L. Pinello. 2018. Integrated design, execution, and analysis of arrayed and pooled CRISPR genome-editing experiments. *Nat. Protoc.* 13:946–986. https://doi.org/10.1038/nprot.2018.005

Carr, C.M., and J. Rizo. 2010. At the junction of SNARE and SM protein function. *Curr. Opin. Cell Biol.* 22:488–495. https://doi.org/10.1016/j.ceb.2010.04.006

Cheung, P.Y., and S.R. Pfeffer. 2016. Transport Vesicle Tethering at the Trans Golgi Network: Coiled Coil Proteins in Action. *Front. Cell Dev. Biol.* 4:18. https://doi.org/10.3389/fcell.2016.00018

Chia, J., G. Goh, V. Racine, S. Ng, P. Kumar, and F. Bard. 2012. RNAi screening reveals a large signaling network controlling the Golgi apparatus in human cells. *Mol. Syst. Biol.* 8:629. https://doi.org/10.1038/msb.2012.59

Chiritoiu, M., N. Brouwers, G. Turacchio, M. Pirozzi, and V. Malhotra. 2019. GRASP55 and UPR Control Interleukin-1β Aggregation and Secretion. *Dev. Cell.* 49:145–155.e4. https://doi.org/10.1016/j.devcel.2019.02.011

Cole, N.B., N. Sciaky, A. Marotta, J. Song, and J. Lippincott-Schwartz. 1996. Golgi dispersal during microtubule disruption: regeneration of Golgi stacks at peripheral endoplasmic reticulum exit sites. *Mol. Biol. Cell.* 7:631–650. https://doi.org/10.1091/mbc.7.4.631

Cruz-Garcia, D., V. Malhotra, and A.J. Curwin. 2018. Unconventional protein secretion triggered by nutrient starvation. *Semin. Cell Dev. Biol.* 83:22–28. https://doi.org/10.1016/j.semcdb.2018.02.021

Dao, D., A.N. Fraser, J. Hung, V. Ljosa, S. Singh, and A.E. Carpenter. 2016. CellProfiler Analyst: interactive data exploration, analysis and classification of large biological image sets. *Bioinformatics.* 32:3210–3212. https://doi.org/10.1093/bioinformatics/btw390

Díaz Añel, A.M., and V. Malhotra. 2005. PKCeta is required for beta1gamma2/beta3gamma2- and PKD-mediated transport to the cell surface and the organization of the Golgi apparatus. *J. Cell Biol.* 169:83–91. https://doi.org/10.1083/jcb.200412089

Duan, R.-D., Y. Cheng, G. Hansen, E. Hertervig, J.-J. Liu, I. Syk, H. Sjöström, and A. Nilsson. 2003. Purification, localization, and expression of human intestinal alkaline sphingomyelinase. *J. Lipid Res.* 44:1241–1250. https://doi.org/10.1194/jlr.M300037-JLR200

Eichel, K., and M. von Zastrow. 2018. Subcellular Organization of GPCR Signaling. *Trends Pharmacol. Sci.* 39:200–208. https://doi.org/10.1016/j.tips.2017.11.009

Finn, R.D., P. Coggill, R.Y. Eberhardt, S.R. Eddy, J. Mistry, A.L. Mitchell, S.C. Potter, M. Punta, M. Qureshi, A. Sangrador-Vegas, et al. 2016. The Pfam protein families database: towards a more sustainable future. *Nucleic Acids Res.* 44(D1):D279–D285. https://doi.org/10.1093/nar/gkv1344

Gilbert, L.A., M.H. Larson, L. Morsut, Z. Liu, G.A. Brar, S.E. Torres, N. Stern-Ginossar, O. Brandman, E.H. Whitehead, J.A. Doudna, et al. 2013. CRISPR-mediated modular RNA-guided regulation of transcription in eukaryotes. *Cell.* 154:442–451. https://doi.org/10.1016/j.cell.2013.06.044

Gilbert, L.A., M.A. Horlbeck, B. Adamson, J.E. Villalta, Y. Chen, E.H. Whitehead, C. Guimaraes, B. Panning, H.L. Ploegh, M.C. Bassik, et al. 2014. Genome-Scale CRISPR-Mediated Control of Gene Repression and Activation. *Cell.* 159:647–661. https://doi.org/10.1016/j.cell.2014.09.029

Guo, Y., D.W. Sirkis, and R. Schekman. 2014. Protein sorting at the trans-Golgi network. *Annu. Rev. Cell Dev. Biol.* 30:169–206. https://doi.org/10.1146/annurev-cellbio-100913-013012

Horlbeck, M.A., L.A. Gilbert, J.E. Villalta, B. Adamson, R.A. Pak, Y. Chen, A.P. Fields, C.Y. Park, J.E. Corn, M. Kampmann, and J.S. Weissman. 2016a. Compact and highly active next-generation libraries for CRISPR-mediated gene repression and activation. *eLife.* 5:e19760. https://doi.org/10.7554/eLife.19760

Horlbeck, M.A., L.B. Witkowsky, B. Guglielmi, J.M. Replogle, L.A. Gilbert, J.E. Villalta, S.E. Torigoe, R. Tjian, and J.S. Weissman. 2016b. Nucleosomes impede Cas9 access to DNA in vivo and in vitro. *eLife.* 5:e12677. https://doi.org/10.7554/eLife.12677

Huebers, H.A., and C.A. Finch. 1987. The physiology of transferrin and transferrin receptors. *Physiol. Rev.* 67:520–582. https://doi.org/10.1152/physrev.1987.67.2.520

Huttlin, E.L., L. Ting, R.J. Bruckner, F. Gebreab, M.P. Gygi, J. Szpyt, S. Tam, G. Zarraga, G. Colby, K. Baltier, et al. 2015. The BioPlex Network: A Systematic Exploration of the Human Interactome. *Cell.* 162:425–440. https://doi.org/10.1016/j.cell.2015.06.043

Huttlin, E.L., R.J. Bruckner, J.A. Paulo, J.R. Cannon, L. Ting, K. Baltier, G. Colby, F. Gebreab, M.P. Gygi, H. Parzen, et al. 2017. Architecture of the human interactome defines protein communities and disease networks. *Nature.* 545:505–509. https://doi.org/10.1038/nature22366

Jin, M., and M.D. Snider. 1993. Role of microtubules in transferrin receptor transport from the cell surface to endosomes and the Golgi complex. *J. Biol. Chem.* 268:18390–18397.

Johannes, L., and V. Popoff. 2008. Tracing the retrograde route in protein trafficking. *Cell.* 135:1175–1187. https://doi.org/10.1016/j.cell.2008.12.009

Kampmann, M. 2018. CRISPRi and CRISPRa Screens in Mammalian Cells for Precision Biology and Medicine. *ACS Chem. Biol.* 13:406–416. https://doi.org/10.1021/acschembio.7b00657

Krogh, A., B. Larsson, G. von Heijne, and E.L.L. Sonnhammer. 2001. Predicting transmembrane protein topology with a hidden Markov model: application to complete genomes. *J. Mol. Biol.* 305:567–580. https://doi.org/10.1006/jmbi.2000.4315

Lee, M.C.S., E.A. Miller, J. Goldberg, L. Orci, and R. Schekman. 2004. Bi-directional protein transport between the ER and Golgi. *Annu. Rev. Cell Dev. Biol.* 20:87–123. https://doi.org/10.1146/annurev.cellbio.20.010403.105307

Li, W., H. Xu, T. Xiao, L. Cong, M.I. Love, F. Zhang, R.A. Irizarry, J.S. Liu, M. Brown, and X.S. Liu. 2014. MAGeCK enables robust identification of essential genes from genome-scale CRISPR/Cas9 knockout screens. *Genome Biol.* 15:554. https://doi.org/10.1186/s13059-014-0554-4

Lippincott-Schwartz, J., L.C. Yuan, J.S. Bonifacino, and R.D. Klausner. 1989. Rapid redistribution of Golgi proteins into the ER in cells treated with brefeldin A: evidence for membrane cycling from Golgi to ER. *Cell.* 56:801–813. https://doi.org/10.1016/0092-8674(89)90685-5

Lopes-da-Silva, M., J.J. McCormack, J.J. Burden, K.J. Harrison-Lavoie, F. Ferraro, and D.F. Cutler. 2019. A GBF1-Dependent Mechanism for Environmentally Responsive Regulation of ER-Golgi Transport. *Dev. Cell.* 49:786–801.e6. https://doi.org/10.1016/j.devcel.2019.04.006

Lorente-Rodríguez, A., and C. Barlowe. 2011. Entry and exit mechanisms at the cis-face of the Golgi complex. *Cold Spring Harb. Perspect. Biol.* 3:a005207. https://doi.org/10.1101/cshperspect.a005207

Luini, A., and S. Parashuraman. 2016. Signaling at the Golgi: sensing and controlling the membrane fluxes. *Curr. Opin. Cell Biol.* 39:37–42. https://doi.org/10.1016/j.ceb.2016.01.014

Ma, T., B. Li, R. Wang, P.K. Lau, Y. Huang, L. Jiang, R. Schekman, and Y. Guo. 2018. A mechanism for differential sorting of the planar cell polarity proteins Frizzled6 and Vangl2 at the *trans*-Golgi network. *J. Biol. Chem.* 293:8410–8427. https://doi.org/10.1074/jbc.RA118.001906

Malhotra, V., and P. Erlmann. 2015. The pathway of collagen secretion. *Annu. Rev. Cell Dev. Biol.* 31:109–124. https://doi.org/10.1146/annurev-cellbio-100913-013002

Mardones, G.A., C.M. Snyder, and K.E. Howell. 2006. Cis-Golgi matrix proteins move directly to endoplasmic reticulum exit sites by association with tubules. *Mol. Biol. Cell.* 17:525–538. https://doi.org/10.1091/mbc.e05-05-0447

Menzies, S.A., N. Volkmar, D.J. van den Boomen, R.T. Timms, A.S. Dickson, J.A. Nathan, and P.J. Lehner. 2018. The sterol-responsive RNF145 E3 ubiquitin ligase mediates the degradation of HMG-CoA reductase together with gp78 and Hrd1. *eLife.* 7:e40009. https://doi.org/10.7554/eLife.40009

Misumi, Y., Y. Misumi, K. Miki, A. Takatsuki, G. Tamura, and Y. Ikehara. 1986. Novel blockade by brefeldin A of intracellular transport of secretory proteins in cultured rat hepatocytes. *J. Biol. Chem.* 261:11398–11403. https://doi.org/10.1016/j.otohns.2008.12.029

Novick, P., C. Field, and R. Schekman. 1980. Identification of 23 complementation groups required for post-translational events in the yeast secretory pathway. *Cell.* 21:205–215. https://doi.org/10.1016/0092-8674(80)90128-2

Park, R.J., T. Wang, D. Koundakjian, J.F. Hultquist, P. Lamothe-Molina, B. Monel, K. Schumann, H. Yu, K.M. Krupzcak, W. Garcia-Beltran, et al. 2017. A genome-wide CRISPR screen identifies a restricted set of HIV host dependency factors. *Nat. Genet.* 49:193–203. https://doi.org/10.1038/ng.3741

Parnas, O., M. Jovanovic, T.M. Eisenhaure, R.H. Herbst, A. Dixit, C.J. Ye, D. Przybylski, R.J. Platt, I. Tirosh, N.E. Sanjana, et al. 2015. A Genome-wide CRISPR Screen in Primary Immune Cells to Dissect Regulatory Networks. *Cell.* 162:675–686. https://doi.org/10.1016/j.cell.2015.06.059

Raote, I., M. Ortega-Bellido, A.J. Santos, O. Foresti, C. Zhang, M.F. Garcia-Parajo, F. Campelo, and V. Malhotra. 2018. TANGO1 builds a machine for collagen export by recruiting and spatially organizing COPII, tethers and membranes. *eLife.* 7:e32723. https://doi.org/10.7554/eLife.32723

Rios, R.M., and M. Bornens. 2003. The Golgi apparatus at the cell centre. *Curr. Opin. Cell Biol.* 15:60–66. https://doi.org/10.1016/S0955-0674(02)00013-3

Rothman, J.E., and L. Orci. 1992. Molecular dissection of the secretory pathway. *Nature.* 355:409–415. https://doi.org/10.1038/355409a0

Saito, K., M. Chen, F. Bard, S. Chen, H. Zhou, D. Woodley, R. Polischuk, R. Schekman, and V. Malhotra. 2009. TANGO1 facilitates cargo loading at endoplasmic reticulum exit sites. *Cell.* 136:891–902. https://doi.org/10.1016/j.cell.2008.12.025

Shalem, O., N.E. Sanjana, E. Hartenian, X. Shi, D.A. Scott, T.S. Mikkelsen, D. Heckl, B.L. Ebert, D.E. Root, J.G. Doench, and F. Zhang. 2014. Genome-scale CRISPR-Cas9 knockout screening in human cells. *Science.* 343:84–87. https://doi.org/10.1126/science.1247005

Shalem, O., N.E. Sanjana, and F. Zhang. 2015. High-throughput functional genomics using CRISPR-Cas9. *Nat. Rev. Genet.* 16:299–311. https://doi.org/10.1038/nrg3899

Simpson, J.C., B. Joggerst, V. Laketa, F. Verissimo, C. Cetin, H. Erfle, M.G. Bexiga, V.R. Singan, J.K. Hériché, B. Neumann, et al. 2012. Genome-wide RNAi screening identifies human proteins with a regulatory function in the early secretory pathway. *Nat. Cell Biol.* 14:764–774. https://doi.org/10.1038/ncb2510

Snider, M.D., and O.C. Rogers. 1985. Intracellular movement of cell surface receptors after endocytosis: resialylation of asialo-transferrin receptor in human erythroleukemia cells. *J. Cell Biol.* 100:826–834. https://doi.org/10.1083/jcb.100.3.826

Söllner, T., and J.E. Rothman. 1994. Neurotransmission: harnessing fusion machinery at the synapse. *Trends Neurosci.* 17:344–348. https://doi.org/10.1016/0166-2236(94)90178-3

Stanley, A.C., and P. Lacy. 2010. Pathways for cytokine secretion. *Physiology (Bethesda).* 25:218–229. https://doi.org/10.1152/physiol.00017.2010

Stewart, S.A., D.M. Dykxhoorn, D. Palliser, H. Mizuno, E.Y. Yu, D.S. An, D.M. Sabatini, I.S.Y. Chen, W.C. Hahn, P.A. Sharp, et al. 2003. Lentivirus-delivered stable gene silencing by RNAi in primary cells. *RNA.* 9:493–501. https://doi.org/10.1261/rna.2192803

Stewart, S.E., S.A. Menzies, S.J. Popa, N. Savinykh, A. Petrunkina Harrison, P.J. Lehner, and K. Moreau. 2017. A genome-wide CRISPR screen reconciles the role of N-linked glycosylation in galectin-3 transport to the cell surface. *J. Cell Sci.* 130:3234–3247. https://doi.org/10.1242/jcs.206425

Tsuboi, K., N. Takezaki, and N. Ueda. 2007. The N-acylethanolamine-hydrolyzing acid amidase (NAAA). *Chem. Biodivers.* 4:1914–1925. https://doi.org/10.1002/cbdv.200790159

Tusnády, G.E., and I. Simon. 2001. The HMMTOP transmembrane topology prediction server. *Bioinformatics.* 17:849–850. https://doi.org/10.1093/bioinformatics/17.9.849

Valm, A.M., S. Cohen, W.R. Legant, J. Melunis, U. Hershberg, E. Wait, A.R. Cohen, M.W. Davidson, E. Betzig, and J. Lippincott-Schwartz. 2017. Applying systems-level spectral imaging and analysis to reveal the organelle interactome. *Nature.* 546:162–167. https://doi.org/10.1038/nature22369

van Galen, J., F. Campelo, E. Martínez-Alonso, M. Scarpa, J.Á. Martínez-Menárguez, and V. Malhotra. 2014. Sphingomyelin homeostasis is required to form functional enzymatic domains at the trans-Golgi network. *J. Cell Biol.* 206:609–618. https://doi.org/10.1083/jcb.201405009

Villeneuve, J., L. Bassaganyas, S. Lepreux, M. Chiritoiu, P. Costet, J. Ripoche, V. Malhotra, and R. Schekman. 2018. Unconventional secretion of FABP4 by endosomes and secretory lysosomes. *J. Cell Biol.* 217:649–665. https://doi.org/10.1083/jcb.201705047

von Blume, J., J.M. Duran, E. Forlanelli, A.M. Alleaume, M. Egorov, R. Polishchuk, H. Molina, and V. Malhotra. 2009. Actin remodeling by ADF/cofilin is required for cargo sorting at the trans-Golgi network. *J. Cell Biol.* 187:1055–1069. https://doi.org/10.1083/jcb.200908040

Voorhees, R.M., and R.S. Hegde. 2016. Structure of the Sec61 channel opened by a signal sequence. *Science.* 351:88–91. https://doi.org/10.1126/science.aad4992

Wendeler, M.W., J.P. Paccaud, and H.P. Hauri. 2007. Role of Sec24 isoforms in selective export of membrane proteins from the endoplasmic reticulum. *EMBO Rep.* 8:258–264. https://doi.org/10.1038/sj.embor.7400893

Wendler, F., A.K. Gillingham, R. Sinka, C. Rosa-Ferreira, D.E. Gordon, X. Franch-Marro, A.A. Peden, J.P. Vincent, and S. Munro. 2010. A genome-wide RNA interference screen identifies two novel components of the metazoan secretory pathway. *EMBO J.* 29:304–314. https://doi.org/10.1038/emboj.2009.350

Wong, M., and S. Munro. 2014. The specificity of vesicle traffic to the Golgi is encoded in the golgin coiled-coil proteins. *Science.* 346:1256898. https://doi.org/10.1126/science.1256898

Woods, J.W., M. Doriaux, and M.G. Farquhar. 1986. Transferrin receptors recycle to cis and middle as well as trans Golgi cisternae in Ig-secreting myeloma cells. *J. Cell Biol.* 103:277–286. https://doi.org/10.1083/jcb.103.1.277

Wu, H., P. Carvalho, and G.K. Voeltz. 2018. Here, there, and everywhere: The importance of ER membrane contact sites. *Science.* 361:eaan5835. https://doi.org/10.1126/science.aan5835

Zanetti, G., K.B. Pahuja, S. Studer, S. Shim, and R. Schekman. 2012. COPII and the regulation of protein sorting in mammals. *Nat. Cell Biol.* 14:20–28. https://doi.org/10.1038/ncb2390

Zhang, M., and R. Schekman. 2013. Unconventional secretion, unconventional solutions. *Science.* 340:559–561. https://doi.org/10.1126/science.1234740